Neuroblast sensory quiescence depends of vascular cytoneme contacts and sensory neuronal differentiation requires initiation of blood flow

Laura Taberner[1], Aitor Bañón[1] and Berta Alsina[1]*

1-Developmental Biology Unit, Department of Experimental and Health Sciences, Universitat Pompeu Fabra-Parc de Recerca Biomèdica de Barcelona, Dr. Aiguader 88, 08003 Barcelona, Spain

*Author for correspondence, berta.alsina@upf.edu

Running Title: Neurovascular interaction in the sensory niche

Keywords: sensory neurons, vascular, niche, cytoneme, Dll4/Notch, blood flow, zebrafish

Highlights

- Vasculature is part of the cranial sensory ganglia niche and regulates neurogenesis.
- Cytoneme contacts between endothelial cells and sensory neuroblasts are required for neuroblast quiescence.
- Endothelial Dll4 and neuroblast Notch1 signal to regulate the growth of cranial sensory ganglia.
- Initiation of blood flow triggers a transcriptional metabolic switch and sensory neuronal differentiation.

Summary

In many organs, stem cell function depends on the communication with their niche partners. Cranial sensory neurons develop in close proximity to blood vessels, however whether vasculature is an integral component of their niches is yet unknown. Here, two separate, novel roles for vasculature in cranial sensory neurogenesis in zebrafish are uncovered. The first involves precise spatiotemporal endothelial-neuroblast cytoneme contacts and Dll4-Notch signalling to restrain neuroblast proliferation. Secondly, we find that blood flow onset triggers a transcriptional response to modify neuroblast metabolic status and is required for sensory neuron differentiation. In contrast, no role of sensory neurogenesis in vascular development is found, suggesting a unidirectional signalling from vasculature to sensory neuroblasts. Altogether, we demonstrate that the cranial vasculature constitutes a hitherto unrecognized niche component of the sensory ganglia that regulates the pace of their growth and differentiation dynamics.

Introduction

Proper interaction and understanding of our external world depend on specialized sensory organs and neurons from the peripheral nervous system (PNS). The cranial PNS consists of several ganglia with sensory bipolar neurons that transmit external sensory information to the brain. Sensory neurogenesis is achieved by a coordinated sequence of specification, delamination, transit-amplification of progenitors and terminal differentiation events (Alsina

et al., 2003; Begbie et al., 2002; Maier et al., 2014; Schlosser, 2010). Several intrinsic factors such as Igf1, FGFs or neurotrophins participate in the proliferation, innervation and function of cranial ganglia during embryogenesis and adulthood (Bilak et al., 2003; Camarero et al., 2003; Fantetti and Fekete, 2012; Murdoch and Roskams, 2012; Vemaraju et al., 2012). Mutations in some of these factors, therefore result in sensory pathologies, i.e. Igf1 mutations are associated with hearing loss in rodents and humans (Bonapace et al., 2003; Riquelme et al., 2010). The rate of sensory neurogenesis is determined by the balance between multipotent stem cells (SCs) and differentiated sensory neurons and the combination of intrinsic factors and extrinsic cues of their microenvironment.

Recent evidences indicate that multipotent SC function *in vivo* is tightly linked to communication with the components of the microenvironment in which they reside, the so called niche (reviewed in Spradling et al., 2001). Blood vessels have emerged as key participants of SC function in several niches, such as the adult neural, hematopoietic and spermatogonia SC niches. Depending on the context, blood vessels regulate SC quiescence, proliferation and/or differentiation (Palmer et al., 2000; Rafii et al., 2016; Shi and Gronthos, 2003; Yoshida et al., 2007).

The adult brain SC niche is one of the niches in which the blood vessel-neuronal interaction was early revealed and, thus, the signals and mechanisms are well understood. There, two types of neurovascular interactions take place, one mediated by direct cell-cell contacts through neural SCs (NSCs) endfeet enwrapping endothelial cells (ECs) (Kacem et al., 1998) and the other mediated by secreted signals from ECs (Shen et al., 2008; Tavazoie et al., 2008)(Mirzadeh et al., 2008; Palmer et al., 2000; Shen et al., 2008; Tavazoie et al., 2008). Cell-cell contact signalling by EphrinB2 and Jagged1 expressed in ECs and, Eph and Notch receptors in NSCs, regulates NSCs quiescence (Ottone et al., 2014). On the other hand, endothelia secrete VEGFs, Angiopoietins, BDNF, NT-3 and PEDF that control NSC self-renewal, progenitor cell proliferation or differentiation (Androutsellis-Theotokis et al., 2009; Calvo et al., 2011; Delgado et al., 2014; Jin et al., 2002a; Louissaint et al., 2002; Ramírez-Castillejo et al., 2006)(Androutsellis-Theotokis et al., 2009; Calvo et al., 2011; Delgado et al., 2014; Jin et al., 2002b; Louissaint et al., 2002; Ramírez-Castillejo et al., 2006). Blood vessels not only communicate through secreted factors, but also by the perfusion of oxygen and nutrients. Oxygen tension mediates the metabolic switch from glycolysis to Oxidative Phosphorylation (OxPhos), which has been shown recently to control NSC fate (Ito and Suda, 2014; Llorens-Bobadilla et al., 2015). In the embryo, vasculogenesis and neurogenesis are spatiotemporally coupled in the central nervous system (Hogan et al., 2004; Ulrich et al., 2011; Vasudevan et

103 al., 2008), but only few studies have addressed the molecular mechanisms underlaying this
104 neurovascular interaction (Lange et al., 2016; Tan et al., 2016; Tata et al., 2016).
105 Cranial ganglia in vertebrates lie in very close proximity to head blood vessels (Taberner et al.,
106 2018), suggesting that vasculature might be an essential component of their niche.
107 Notwithstanding, this question and the mechanisms involved in their communication remain
108 to be addressed in the sensory PNS.
109 In this study, by taking advantage of an avascular model and double labelling of ECs and
110 sensory neurons in zebrafish, we identify two distinct mechanisms by which vasculature
111 regulates cranial sensory neurogenesis. *In vivo* imaging of the developing sensory ganglia
112 reveals that ECs and neuroblasts establish direct contacts through filopodial protrusions.
113 Inhibition of the filopodial contacts show that they exert signalling functions over sensory
114 neuroblast. Thus, the work establishes first evidences for neurovascular interaction mediated
115 by cytonemes. Genetic and pharmacological perturbations show that cytoneme contacts and
116 Dll4 signalling inhibit neuroblasts cell cycle entry and regulate quiescence at early timepoints.
117 Later, blood flow initiation activates a transcriptional program linked to oxygen sensing by
118 Egln2 and a metabolic switch to OxPhos, together with the promotion of cranial ganglia
119 differentiation. Our results uncover, for the first time, that the cranial vasculature is an
120 essential component of the sensory ganglia niche and can temporally regulate neuroblast
121 quiescence and differentiation by using distinct signalling mechanisms.
122

123 ## Results

124 **Vasculature regulates the number of SAG neuroblasts by restraining cell cycle entry of**
125 **neuroblasts**

126 We focused on neurovascular interactions in the statoacoustic ganglion (SAG), which comprise
127 the sensory neurons that innervate mechanosensory hair cells of the inner ear and the
128 brainstem. During neurogenesis, *neurog1*$^{+}$ neuronal precursors (blue) transit into neurod^{+}
129 neuroblasts (green) that delaminate and coalesce into the SAG. Later they differentiate into
130 Islet2^{+} neurons (orange) (Figure 1A). The developing zebrafish SAG lies between three main
131 vessels, the Primordial Hindbrain Channel (PHBC) that runs between the hindbrain and the
132 otic vesicle (OV), the Lateral Dorsal Aorta (LDA) beneath the OV and the Primary Head Sinus
133 (PHS) surrounding laterally the OV (Taberner et al., 2018) (Figure 1B).
134 To functionally evaluate if cranial vasculature regulates the development of cranial sensory
135 neurons in SAG, we analysed SAG growth dynamics in *cloche* (*clo*) homozygous mutants in the
136 double *TgBAC(neurod:EGFP)* ^{nl1}*;(Kdrl:ras-mCherry)* ^{s896} background, in which eGFP marks

137 sensory neurons and mCherry marks ECs. *Cloche* encodes *npas4l*, a PAS-domain-containing
138 bHLH transcription factor required for the formation of endothelial and hematopoietic cells
139 (Reischauer et al., 2016; Stainier et al., 1995) and *clo* mutants have extensively been used as
140 an avascular model (Liao et al., 1997; Sumanas et al., 2005). In *clo* mutant embryos, the SAG
141 appeared larger compared to siblings (sib) at 36 and 72 hpf (Figure 1C). Quantification of SAG
142 volumes revealed a statistically significant increase in *clo* mutant embryos (Figure 1D).
143 Moreover, the SAG displayed an abnormal shape and a significant expansion along its
144 mediolateral axis but not along the anteroposterior or dorsoventral axis (Figures 1C and 1E).
145 The increased volume in *clo* mutant embryos could reflect a loss of confinement of the SAG
146 cells by taking the space left by the lack of blood vessels or, alternatively, a higher number of
147 Neurod$^+$ cells. To distinguish between both possibilities, we quantified in serial transverse
148 sections the nuclei within the GFP-labelled SAG cells between 30 to 72 hpf in the *clo* mutant
149 and sibling embryos (Figures 1F and S1). In siblings, there is a period of steep SAG growth
150 between 30 to 36 hpf, (sib 30 hpf: 89 ± 5; sib 36 hpf: 128 ± 5). From 36 to 72 hpf, the mean
151 number of Neurod$^+$ cells is 105 ± 8, suggesting that after 36 hpf this population does not grow.
152 Remarkably, we found that the number of Neurod$^+$ cells was significantly higher in *clo* mutant
153 embryos compared to siblings at 36 hpf (sib: 128 ± 5 vs *clo*$^{-/-}$: 177 ± 5) and this increase
154 persisted at all the following timepoints (Figure 1F). Several mechanisms could account for
155 the increased number of Neurod$^+$ cells in *clo* mutant embryos: i) increased specification of
156 *neurog1*$^+$ cells within the otic epithelium and thereby increased delamination of Neurod$^+$ cells,
157 ii) reduced differentiation of Neurod$^+$ cells into Islet2$^+$ neurons or iii) increased proliferation
158 of the transit-amplifying Neurod$^+$ population. We did not find a higher number of *neurog1*$^+$-
159 expressing cells in the otic epithelium in *clo* mutant embryos compared to siblings (Figures 1G
160 and 1G') nor significant differences in the number of differentiated Islet2$^+$ cells in the SAG
161 (Figures 1H and 1H'). Instead, in *clo* mutant embryos we detected a significantly higher
162 number of proliferating Neurod$^+$ cells after a BrdU pulse from 24 to 30 hpf (expressed as
163 BrdU$^+$/Neurod$^+$ ratio) (Figures 1I and 1I').
164 Hence, our results show that at early timepoints, cranial vasculature regulates the number of
165 SAG neuroblasts by negatively controlling cell proliferation of Neurod$^+$ cells and therefore
166 constitutes an essential component of the neurosensory niche during development.
167
168 **Cranial blood vessels and sensory neuroblasts establish direct contacts through filopodia**
169 In both the embryonic and adult brain, NSCs establish contacts with ECs through endfeet
170 projections (Ottone et al., 2014; Tan et al., 2016; Tavazoie et al., 2008). Therefore, we

171 wondered if neuroblasts from the SAG also establish direct contacts with the adjacent vessels.
172 To investigate this in detail, we live-imaged sensory neuroblasts from the SAG and ECs from
173 the PHBC in double *TgBAC(neurod:EGFP)* ^{nl1}*;(Kdrl:ras-mCherry)* ^{s896} reporter lines, at high
174 spatiotemporal resolution. At 30 hpf, we did not observe neuronal extensions enwrapping
175 ECs of the PHBC, but instead observed dynamic, thin filopodia extending from ECs to Neurod^{+}
176 cells, as well as similar filopodia from Neurod^{+} cells extending to ECs (Figures 2A, 2B, S2, S3
177 and Supplemental Movies S1-4). The dynamics of filopodia were varied; in some instances, we
178 observed filopodia extending and retracting in seconds (Figures 2A and 2B, cyan and magenta
179 arrowheads respectively), in others, filopodia remained stable for several minutes (Figures 2A
180 and 2B, yellow arrowheads). Interestingly, some PHBC filopodia did not remain at the surface
181 of the SAG but contacted deeper neuroblast somas (Supplemental Movie S4). Moreover,
182 stable filopodia-filopodia contacts between neuroblasts and ECs were also seen in some cases
183 (Figures 2C and S3). As observed in transverse optical confocal reconstructions of the vessels
184 and the SAG, filopodia were highly directional: PHBC filopodia extended only ventrally in the
185 direction of sensory Neurod^{+} cells (Figures 2D and 2E). Interestingly, filopodia were present
186 from 24 to 36 hpf but not later, suggesting an early role of filopodia in vessel-neuroblast
187 communication (Figure 2F). Altogether, highly directed and temporally regulated filopodia-
188 mediated cell contacts are established between both EC and sensory neuroblasts.
189
190 **Sensory neurons are not required for cranial vascular patterning**
191 Communication between neurons and vessels in the CNS can take place from vessels to
192 neurons, vice-versa and bidirectionally (Barber et al., 2018; Makita et al., 2008; Mukouyama
193 et al., 2002). Thus, we next investigated if sensory neuron development has a role in vascular
194 patterning near sensory ganglia. In this case, we analysed homozygous *neurog1*^{hi1059} mutant
195 embryos -which fail to specify sensory neuronal precursors (Ma et al., 1998)- in the double
196 transgenic *TgBAC(neurod:EGFP)* ^{nl1}*;(Kdrl:ras-mCherry)* ^{s896} reporter line. Strikingly, despite the
197 total absence of SAG and other cranial ganglia in *neurog1* mutant embryos, development of
198 the PHBC and LDA displayed no obvious patterning defects at 30 hpf (Figure 3A). The central
199 arteries (CtAs) ingrowth into the hindbrain also did not display any delay nor obvious
200 alteration at 48 hpf (Figure 3A). We quantified the width of PHBC and the number of ECs at
201 48 hpf, and again found no significant differences between *neurog1* mutants and siblings
202 (Figures 3B and 3C). In conclusion, our data indicate that cranial vascular development does
203 not require signals from sensory neuroblasts and suggest that primarily the signalling direction
204 goes from vessels to neurons.

205 Since imaging revealed directed filopodial contacts from cranial vessels to sensory neurons
206 and vice-versa (Figure 2A), we wondered about possible growth interdependency. We imaged
207 neuronal filopodia dynamics in the absence of vessels and, endothelial filopodia in the
208 absence of neurons. In *clo* mutants, the number of neuronal filopodia was drastically reduced
209 (Figures 3D and 3D'). In contrast, in *neurog1* mutant embryos the number of ECs filopodia did
210 not change, though they were shorter (Figures 3E and 3E''). These data indicate that signals
211 from ECs are required for neuronal filopodia formation.
212 While sensory neurons in SAG do not appear to be required for vascular development, our
213 data indicate that vasculature is required for SAG neurons to proliferate during a temporal
214 window that coincides with the period of filopodial contacts. Moreover, neuroblasts only
215 extend filopodia when ECs are present. Altogether, the results support the hypothesis that
216 endothelial-neuronal filopodia contacts are required for vessels to signal to neuroblasts in the
217 SAG to restrict growth.
218
219 **Cell signalling mediated by cytonemes regulates the number of SAG neuroblasts**
220 Cell signalling through filopodia has emerged as a novel mechanism of signalling between
221 adjacent cells in different embryonic tissues (Kornberg, 2017; Stanganello and Scholpp, 2016;
222 Stanganello et al., 2015). Signalling filopodia have been named cytonemes (Ramírez-Weber
223 and Kornberg, 1999). In order to assess the possible role of filopodial signalling in SAG growth,
224 filopodia formation was inhibited with LatrunculinB (LatB), a toxin that binds to actin and has
225 been used to impair filopodia function *in vivo* (Morton et al., 2000; Phng et al., 2013). Imaging
226 and quantification of filopodia in embryos treated with LatB for 6 hours indicated that the
227 treatment was effective, the number of filopodia in ECs and in neuroblasts was reduced
228 (Figures 4A and 4B). Interestingly, inhibition of filopodia caused an increased number of
229 Neurod^{+} cells in LatB-treated embryos (Figure 4C) and this phenotype was also due to a higher
230 number of Neurod^{+} cells incorporating BrdU (Figures 4D and 4E). No additional effects were
231 found in treated *clo* mutant embryos, indicating specific effects of neuroblasts (Figure 4C).
232 Hence, filopodia formation inhibition at early stages recapitulated the SAG growth phenotype
233 found previously in the avascular mutant. These data demonstrate that the endothelial-
234 neuronal filopodial contacts are cytonemes exerting a signalling role onto SAG neuroblast
235 proliferation.
236
237
238

239 **Dll4 inhibition increases the Neurod$^+$ population**

240 To identify signals that could mediate the neurovascular crosstalk we revisited the published
241 vascular signals regulating CNS neurogenesis for evidence of ligand expression in cranial
242 vasculature and their receptors in cranial sensory neurons (Howe et al., 2013). In the
243 Ventricular-Subventricular Zone (V-SVZ) of the adult brain, endothelial Jagged1 ligand
244 restrains NSC proliferation (Ottone et al., 2014). Cranial vessels do not express Jagged1 but do
245 express Delta-like 4 (Dll4) (Fujita et al., 2011), another Notch ligand, which is essential for
246 proper vascular remodelling and sprouting (Bussmann et al., 2011; Leslie et al., 2007;
247 Siekmann and Lawson, 2007). We therefore hypothesized that Dll4 could be signalling to SAG
248 neurons, which express Notch1 at the same early timepoints (Nikolaou et al., 2009).
249 Moreover, it has been postulated that pigmentation patterning in zebrafish is regulated by
250 DeltaC-Notch signalling through filopodia (Hamada et al., 2014).

251 To test this hypothesis, we inhibited *dll4* through the well-studied *dll4* morpholino (MO)
252 (Bussmann et al., 2011; Siekmann and Lawson, 2007) and assessed its effects on SAG growth.
253 Remarkably, *dll4* morphant embryos presented an expansion of the Neurod$^+$ population
254 similar to the one observed previously in *clo* mutant embryos (Figure 5A). This expansion was
255 reflected both in SAG volume (Fig 5B) as well as in Neurod$^+$ cell number (Figure 5C). As a
256 further control, *dll4* morpholino was also injected in *clo* mutant embryos and the number of
257 Neurod$^+$ cells did not change, suggesting that the results are due to loss of *dll4* expressed by
258 the vasculature (Figures 5A-5C). These findings reveal that Dll4 is required to regulate Neurod$^+$
259 cell number.

260 In angiogenic sprouts, the number of filopodia increases after *dll4* downregulation (Suchting
261 et al., 2007). When we assessed the number of filopodia in the developed PHBC, we detected
262 a small increase in filopodial number and no differences in their length (Figures 5D-5F). Thus,
263 the increase of Neurod$^+$ cells in *dll4* morphants cannot be attributed to a lack of filopodial
264 processes but to a specific lack of signal. Finally, the number of ECs did not change in *dll4*
265 morphant embryos compared to embryos injected with a random morpholino (Figures 5G and
266 5H). Therefore, the increase in Neurod$^+$ cell number after *dll4* down-regulation is not due to
267 vascular developmental changes but to Dll4-Notch1 signalling.

268 Together, these results suggest that Dll4 signalling constitutes one of the key molecular
269 mechanisms by which the vasculature regulates cranial sensory neurogenesis.

270

271

272

273 **Absence of vasculature impairs sensory neuronal differentiation**

274 Since more neuroblasts form in the SAG in the absence of vasculature, we next assessed if
275 these neuroblasts differentiate, resulting in a higher number of Islet2$^+$ post-mitotic cells at
276 later stages. Unexpectedly we found, after plotting the number of immunostained Islet2$^+$
277 nuclei from 30 to 96 hpf, that there was a significantly lower number of Islet2$^+$ cells in *clo*
278 mutants from 54 hpf onwards (Figures 6A and 6B). The differentiation curves indicate that,
279 while at early timepoints sensory differentiation occurs partially independently of vasculature,
280 from 54 hpf onwards, cranial vasculature is required to promote differentiation of Neurod$^+$
281 cells to Islet2$^+$ cells. As expected from the immunostaining data, the fluorescence from sensory
282 axons was also reduced in *clo* mutant embryos, labelled by the *Tg(isl2:GFP)* ^{zc7} reporter line
283 which marks *in vivo* the cytoplasm of differentiated sensory neurons (Pittman et al., 2008)
284 (Figure 6C).

285 To determine if cranial vasculature regulates neurogenesis in other sensory ganglia besides
286 the SAG, we assessed for filopodia contacts and quantified the number of Neurod$^+$ and Islet2$^+$
287 cells in different ganglia. Here, we did not perform a temporal analysis, but we chose discrete
288 timepoints. At 30 hpf, we could also detect filopodia from the PHBC to the trigeminal and
289 anterior lateral line ganglia (Figure S4C). At 36 hpf, we found a significantly increased number
290 of Neurod$^+$ cells in the trigeminal ganglion of *clo* mutants (Figures S4A and S4B), whereas at
291 72 hpf there was a reduced number of Islet2$^+$ cells in the trigeminal and vagal ganglia (Figures
292 S3D-S3G). Therefore, the neurovascular interaction appears to extend to other sensory
293 ganglia.

294 To complete the analysis, we assessed if vasculature could regulate the development of other
295 cell types such as the hair cells of the inner ear. For this aim, we generated *clo* homozygous
296 mutants in the *Tg(brn3c:mGFP)* ^{s356t} background that labels the membranes of hair cells and
297 their kinocilia (Xiao et al., 2005). Serial confocal stacks taken at 72 hpf and quantification of
298 hair cells did not reveal significant differences in hair cell number in cristae nor maculae of *clo*
299 mutants compared to siblings (Figures 6D-6F). Therefore, vasculature is specifically affecting
300 neuronal differentiation of the inner ear but not hair cell number.

301

302 **Initiation of blood flow and oxygen sensing triggers sensory differentiation**

303 It has been reported that in zebrafish blood flow begins due to the completion of anastomosis
304 of cranial blood vessels around 48 to 60 hpf (Siekmann et al., 2009). The coincidence of this
305 timing with the one of sensory differentiation defects in *clo* mutant embryos prompted us to
306 explore whether the inducing signal of sensory differentiation was linked to blood flow. To

307 this aim, we incubated embryos with Nifedipine, a drug that inhibits heartbeat and blood flow
308 (Li et al., 2008). As expected from blood flow inhibition, we observed a drastic vessel diameter
309 reduction in Nifedipine-treated embryos (Figures 7A and 7B). In embryos treated with
310 Nifedipine from 54 to 72 hpf, the number of Islet2^{+} cells decreased, recapitulating the defects
311 found in *clo* mutant embryos (Figures 7C-7E). Treatment in the avascular model did not further
312 enhance the phenotype, suggesting that the differentiation arrest is mostly attributed to the
313 absence of blood flow in *clo* mutant embryos and not associated to side effects of Nifepidine
314 (Figure 7E). The same results were obtained when treatment was done with BDM, another
315 drug used to inhibit blood flow (Anderson et al., 2008) (Figure S5C and S5D). To narrow down
316 the time window of blood flow requirement, we incubated embryos with Nifedipine from 60
317 to 72 hpf and from 48 to 60 hpf. Incubation from 60 to 72 hpf did not inhibit differentiation
318 (Figures 7F and 7G), whereas incubation from 48 to 60 hpf did (Figures S5A and S5B). These
319 results indicate that blood flow induction of sensory differentiation takes place in a narrow
320 time window and once signalling is initiated, blood flow is no longer required.
321 To obtain insight into the molecular mechanisms underlying the arrest in sensory neuron
322 differentiation in the absence of vasculature, we conducted a transcriptional profiling of
323 freshly sorted Neurod GFP^{+} SAG cells from *clo* mutant and sibling embryos at 54 hpf. RNA-seq
324 analysis revealed a transcriptional profile response in the absence of vasculature with 641
325 genes significantly downregulated and 15 upregulated in clo mutant compared to control
326 embryos (Figure 7H). This suggest that in absence of blood flow some signalling pathways are
327 shut down rather a new transcriptional program being activated, what matches with a cell
328 differentiation arrest. Whereas we expected pathways related to differentiation signals or
329 cell-cycle control being down-regulated, most differentially expressed genes found where
330 genes related with oxygen sensing (egln2), reduction-oxidation (redox) process (rdh8a) and
331 mitochondria metabolism (rmnd1 and abat) (Figures 7H ans 7I). Thus, the first transcriptional
332 response to blood flow onset seems to be related to oxygen sensing and switch from glycolysis
333 to OxPhos that ultimately drives sensory neuronal differentiation, as observed in other
334 contexts (Hawkins et al., 2016; Homem et al., 2014; Kida et al., 2015; Lange et al., 2016; Ryall
335 et al., 2015).
336 Altogether, the results define for the first time a prominent role of cranial vasculature in
337 sensory neurogenesis that can be segregated into two sequential and independent
338 mechanisms. A first one, in which Dll4-Notch1 cytoneme signalling from ECs to neurons
339 regulates neuroblast quiescence, and a second one in which initiation of blood flow and
340 oxygen sensing induces a metabolic switch and sensory neuron differentiation.

341 ## Discussion

342 The SAG and other cranial sensory ganglia reside in a vascularized milieu in embryos and
343 adults. A fundamental question in developmental neurobiology is whether or not vasculature,
344 in addition to transport of nutrients and oxygen, provides instructive cues for sensory
345 neurogenesis. This is relevant to understand hearing loss and other sensory neuropathies
346 linked to vascular defects (Jensen et al., 2004; Lago et al., 2018; Paul et al., 2016). Our detailed
347 temporal analysis reveals that cranial ganglia indeed require vascular signals for proper
348 growth and differentiation. We identified two segregated mechanisms: an early cytoneme-
349 based, cell-cell contact dependent mechanism regulating neuroblast proliferation and a later
350 blood flow-dependent mechanism controlling neuronal differentiation.

351 In the V-SVZ, quiescent NSCs physically contact blood vessels with specialized endfeet (Kacem
352 et al., 1998). By taking advantage of the imaging and cell reporter tools available in the
353 zebrafish model we resolve, for the first time, that cell-cell communication between
354 vasculature and neuroblasts takes place through dynamic cytoneme extensions that project
355 between them. It is still possible that in other contexts, dynamic contacts also exist, but
356 imaging in fixed tissue might have hampered their identification, as suggested by Obernier
357 and colleagues (Obernier et al., 2018). Filopodia in angiogenic tip cells and migrating ECs have
358 been described (Fantin et al., 2015; Gerhardt et al., 2003; Ochsenbein et al., 2016; Phng et al.,
359 2013). To our knowledge, filopodia from endothelial stalk cells contacting neuronal cells have
360 not been reported before. One could envision cell-cell contact with only ECs extending
361 filopodia to neuronal somas but, in our system, both cell types project directional filopodia.
362 Signalling filopodia or cytonemes in *Drosophila* and vertebrates have been demonstrated,
363 extending the cell-cell signalling distance of influence (Kornberg, 2017; Stanganello and
364 Scholpp, 2016; Stanganello et al., 2015). This is relevant in the facial mesenchyme where
365 vasculature does not grow inside the sensory ganglia but adjacent. Different types of
366 cytoneme contacts have been described in previous studies, in some cases cytonemes contact
367 the cell body of their target cell (Huang and Kornberg, 2015; Stanganello et al., 2015), while in
368 other cases cytoneme-cytoneme contacts are observed (Du et al., 2016; González-Méndez et
369 al., 2017; Huang and Kornberg, 2015; Roy et al., 2014; Sanders et al., 2013). It is difficult to tell
370 if in our system cytoneme-cell body contacts occur, but we have clearly observed cytoneme-
371 cytoneme contacts. These cytonemes have distinct behaviours, either highly transient or more
372 stable, the latter possibly being actively signalling.

373 Moreover, the study highlights the requirement of signals from ECs for neuronal cytoneme
374 growth. By blocking filopodia projections, we demonstrate that they have a signalling function

375 in the negative control of neuroblast cell proliferation. Most likely only a subset of neuroblasts
376 are contacted by endothelial cytonemes, allowing a scattered pattern of cell cycle-arrested
377 neuroblasts between others with proliferative capacities. Cytonemes have been described to
378 participate in stem cell maintenance in *Drosophila* (Fuwa et al., 2015; Inaba et al., 2015;
379 Mandal et al., 2007; Rojas-Ríos et al., 2012), but not yet described to participate in a NSC niche
380 in vertebrates.
381 In contrast to other contexts in which neurons control vascular patterning (Himmels et al.,
382 2017), our results suggest that in the context of sensory ganglia and surrounding vessels, an
383 absence of cranial ganglia does not have a major effect on early vasculogenesis.
384 During adult neurogenesis, cell contact-dependent neurovascular signalling is mediated by
385 ephrinB2 and Jagged1 present in ECs that suppress cell-cycle entry in NSCs (Ottone et al.,
386 2014). We propose that in the PNS Dll4, but not Jagged1, plays a similar role. Maintenance of
387 a quiescent and undifferentiated population of neural progenitors is key for life-long
388 regeneration. Thus, the role we have uncovered for cranial vasculature and Dll4 in the cranial
389 sensory niche might be relevant in regenerative studies upon neuronal damage.
390 Several studies have highlighted the role of blood flow initiation in remodelling the
391 vasculature, VEGF expression, angiogenesis and stimulation of hematopoietic stem cell
392 formation (Adamo et al., 2009; Bussmann et al., 2011; Nicoli et al., 2010). Blood flow can
393 exert tangential and perpendicular forces on ECs leading to actomyosin rearrangements, YAP-
394 TAZ nuclear translocation and the induction of the mechano-sensitive transcription factor
395 Klf2a (Nakajima et al., 2017; Nicoli et al., 2010; Le Noble et al., 2008). Ultimately, blood flow
396 triggers gene transcriptional changes in ECs and vessel maturation (Chiu and Chien, 2011).
397 On the other hand, blood vessels can exert their roles on neural cells via delivery of nutrients
398 or oxygen (Cleaver and Dor, 2012; Ramasamy et al., 2015). The transcriptome analysis of SAG
399 neuroblasts in clo mutant vs control embryos at the timepoint of blood flow initiation allowed
400 us to identify *egln2* (*Egl nine homolog 2*) as one of the early-response genes more differentially
401 expressed. Egln2 is cellular oxygen sensor involved in the degradation of the transcription
402 *factor hypoxia-inducible factor* (*HIF1*) (Epstein et al., 2001), thus in wild-type conditions
403 embryos sense the passage from hypoxic to normoxic conditions. Additionally, genes related
404 to redox state and mitochondria metabolism are also differentially expressed. Our data
405 suggest that SAG sensory precursors switch from glycolytic to OxPhos to induce their
406 differentiation. Numerous populations of multipotent SC, i.e hemaepoietic SC, intestinal crypt
407 SC and neural SC, use a glycolytic program in their niche and switch to OxPhos upon

408 regeneration and differentiation (Cliff and Dalton, 2017; Lange et al., 2016; Mohrin et al.,
409 2015; Shi et al., 2015).
410 Our current work identifies novel mechanisms for head vasculature in the balance between
411 sensory precursor and differentiation fates and shall contribute to our basic understanding of
412 the cranial sensory niche in which head vasculature enters in scene.
413

414 Acknowledgments

415 We thank D Stainer for the *Tg(cloche)* ^{m378} and *Tg(kdrl:ras-mCherry)* ^{s896} lines, the PRBB Imaging
416 Facility and the UPF Genomics Core and Flow Cytometry Facilities for technical support, T.
417 Schilling, A. Bigas and I. Fariñas for comments on the manuscript and lab members for
418 discussions. The work was supported by BFU2014-53203 and BFU2017-82723P from MCINN
419 to BA and the Unidad de Excelencia Maria de Maeztu (MDM-2014-0370).
420

421 Author Contributions

422 LT and BA designed research, LT and AB performed experiments, LT, AB and BA analysed data
423 and TL and BA wrote the manuscript.
424

425 Declaration of Interests

426 The authors declare that they have no conflict of interest.
427

428 Figure Legends

429 **Figure 1 In the absence of vessels, the Neurod^{+} population in the SAG is expanded due to**
430 **increased proliferation but not to effects on specification or differentiation.**

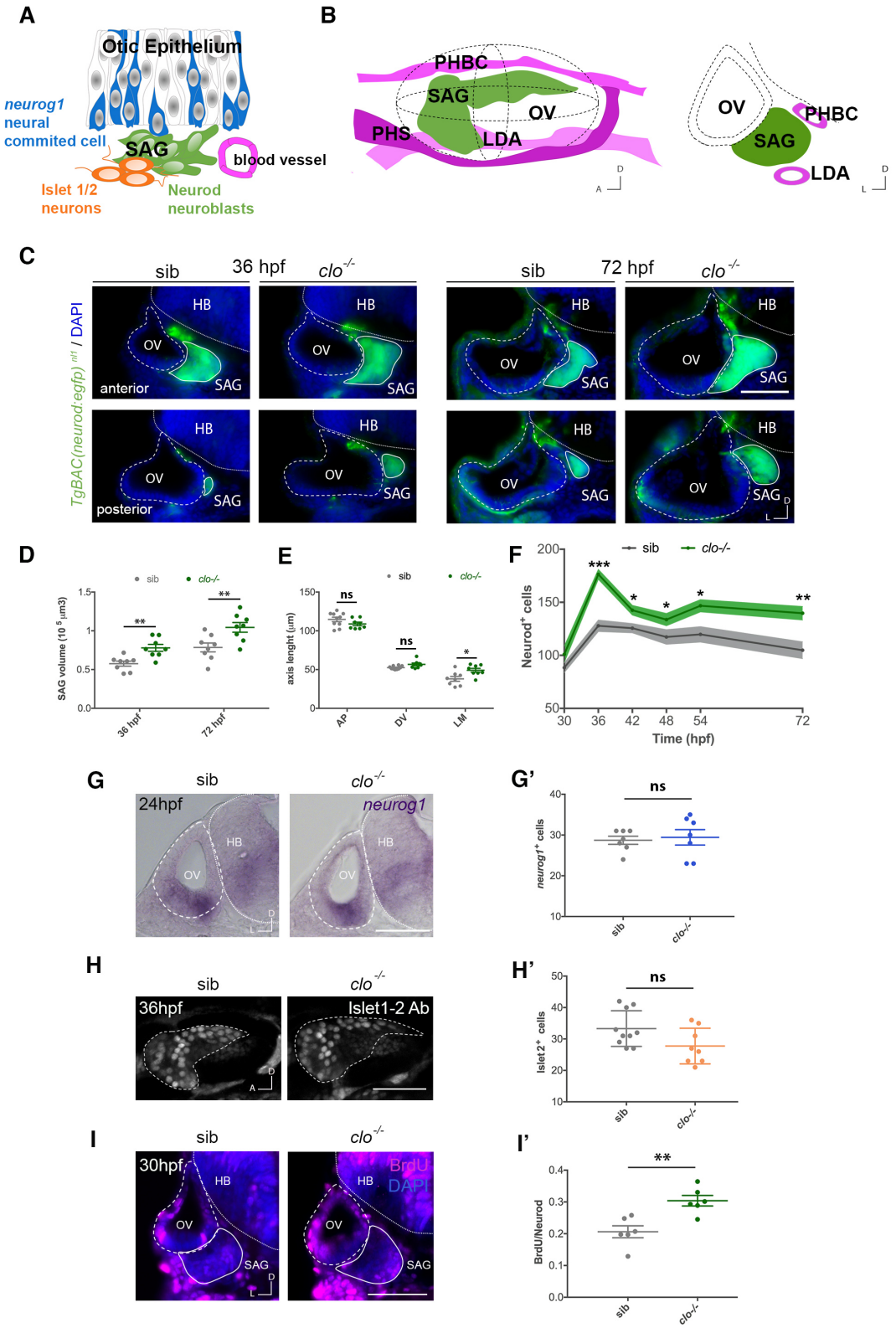

(A) Schematic drawing of the sequential steps of otic neurogenesis. Coloured graphs representing effects in specific cell types will follow this scheme: neurog1^{+} neuronal committed progenitors in blue, Neurod^{+} neuroblasts in green, Islet1/2^{+} neurons in orange and blood vessels in magenta.

436 (B) Lateral (left) and transversal (right) 3D drawing of the OV (dotted line), the SAG and the
437 adjacent vessels: PHBC, LDA and PHS.
438 (C) Representative anterior and posterior transverse images of the SAG in sib and clo$^{-/-}$
439 *TgBAC(neurod:egfp)* ^{nl1} embryos of cryostat sections, at 36 and 72 hpf. Neurod^{+} cells: green,
440 neuroblasts; DAPI: blue, nuclei.
441 (D) Quantification of SAG volumes in sib and clo$^{-/-}$ embryos at 36 and 72 hpf (n=8).
442 (E) Graph showing measurements of the anteroposterior (AP), dorsoventral (DV) or
443 mediolateral (ML) axis length of the SAG in sib and clo$^{-/-}$ embryos (n=8-10), at 72 hpf.
444 (F) Quantification of Neurod^{+} nuclei in the SAG visualized through the *TgBAC(neurod:egfp)* ^{nl1}
445 of sib and clo$^{-/-}$ embryos at different timepoints from 30 to 72 hpf (n = 6-10).
446 (G) Transversal images of *neurog1 in situ* hybridization in the OV epithelium in sib and clo$^{-/-}$
447 embryos, at 24 hpf; and quantified in G' (n = 7).
448 (H) Confocal lateral images of immunostained Islet 1/2^{+} nuclei in the SAG (dotted line,
449 visualized by *TgBAC(neurod:egfp)* ^{nl1}) in sib and clo$^{-/-}$ embryos, at 36 hpf; and quantified in H'
450 (sib n = 10, clo$^{-/-}$ n = 8).
451 (I**)** Transversal images of BrdU incorporation (magenta) in the SAG (continuous line, visualized
452 by *TgBAC(neurod:egfp)* ^{nl1}) in sib and clo$^{-/-}$ embryos, at 30 hpf; and quantified in I' (n = 6). DAPI:
453 blue, nuclei.
454
455 Scale bar, 50 µm. Error bars, mean ± SEM for D,E,G',H',I'; and mean ± SD for F. Unpaired two-
456 tailed Student's *t*-test. * $p < 0.05$, ** $p < 0.01$, *** $p < 0.001$. ns, non-significant. OV, otic
457 vesicle; SAG, statoacoustic ganglion; PHBC, primordial hindbrain channel; LDA, lateral dorsal
458 aorta; PHS, primary head sinus; HB, hindbrain; sib, siblings.
459
460 **Figure 2 Endothelial cells and SAG neuroblasts contact through directional filopodia.**

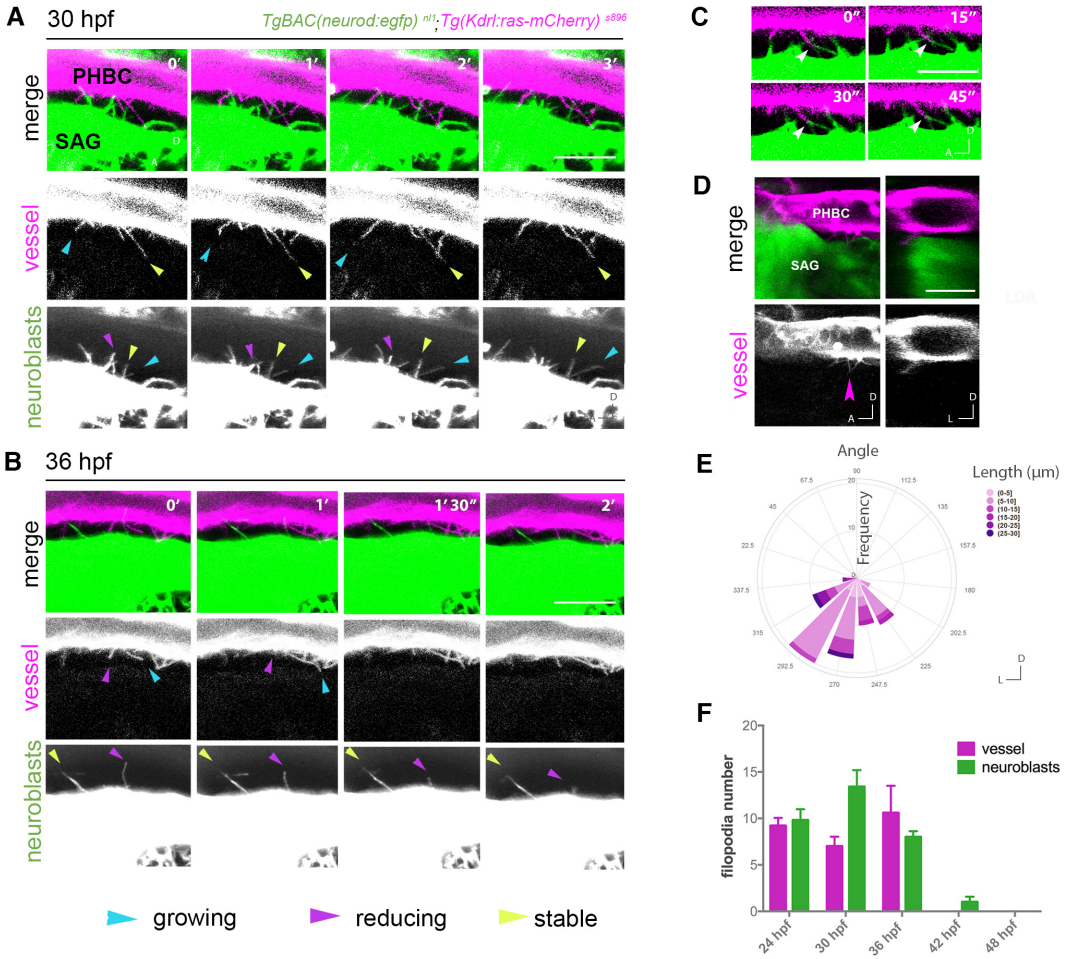

(A,B) Timelapse of lateral images of *TgBAC(neurod:egfp)* ^{nl1}*; (Kdrl:ras-mCherry)* ^{s896} embryos showing filopodia extending from the PHBC to the SAG and from the SAG to the PHBC at 30 and 36 hpf (videos are representative of 5 experiments). Cyan, magenta and yellow arrowheads point to examples of growing, reducing and stable filopodia, respectively.

(C) 4 µm thick z-projection exemplifying a filopodia-filopodia contact remaining stable for more than 45 seconds, 30 hpf.

(D) Single plane images in lateral view and transversal optic reconstruction showing a filopodial process from the PHBC to the SAG, at 30 hpf. Arrowhead indicates point for transverse optical reconstruction.

(E) Rose plot of PHBC filopodia frequency of angle distribution and length (0º, lateral; 90º, dorsal; 180º, medial; 270º, ventral (n=76 filopodia, 15 embryos), at 30 hpf.

(F) Histogram showing the number of filopodia in the PHBC (magenta) and the SAG (green) at different timepoints from 24 to 48 hpf (n = 5).

Scale bars, 20 µm in A,B,D and 10 µm in C. SAG, statoacoustic ganglion; PHBC, primordial hindbrain channel.

Figure 3 Lack of neurogenesis does not affect cranial vasculature patterning nor filopodia formation, while loss of vasculature prevents neuroblasts filopodia formation.

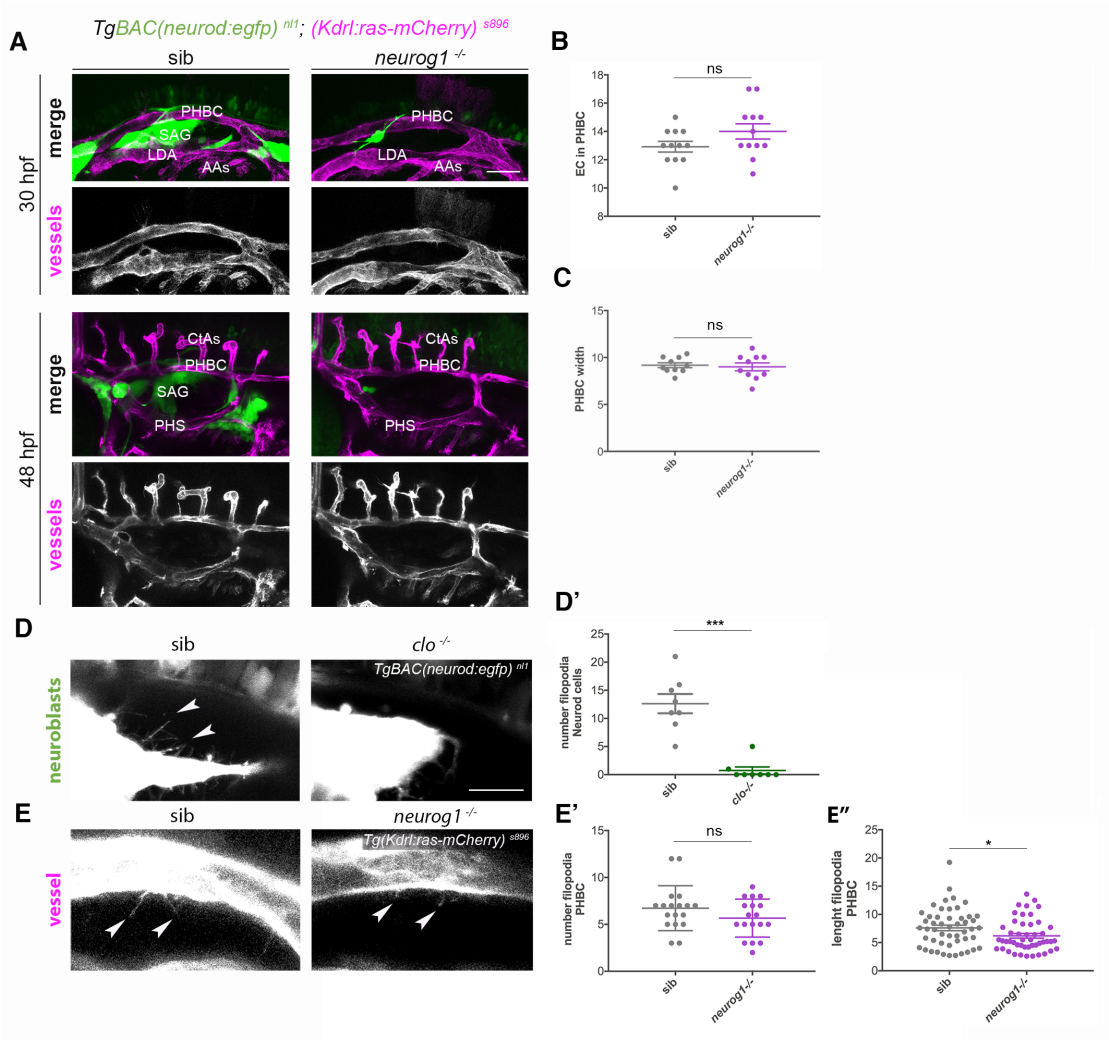

(A) Representative lateral images of cranial vasculature in sib and *neurog1*$^{-/-}$ homozygous mutant embryos in *TgBAC(neurod:egfp)* ^{nls1}, *(Kdrl:ras-mCherry)* ^{s896} background, at 30 hpf and 48 hpf.

(B) Quantification of EC numbers in sib and *neurog1*$^{-/-}$ (n = 12), at 48 hpf.

(C) Quantification of PHBC width in sib and *neurog1*$^{-/-}$ (n = 10), at 48 hpf.

(D) Confocal lateral images showing neuroblasts filopodial processes visualized through the *TgBAC(neurod:egfp)* ^{nl1} in sib and clo $^{-/-}$, at 30 hpf.

(D') Graph of SAG neuroblasts filopodia number in sib and clo $^{-/-}$ (n = 8), at 30 hpf.

(E) Confocal lateral images showing PHBC filopodial processes visualized through the *Tg(Kdrl:ras-mCherry)* ^{s896} in sib and *neurog1*$^{-/-}$ embryos, at 30 hpf. Arrowheads indicate filopodia in D and E.

(E') Graph of PHBC filopodia number in sib and *neurog1*$^{-/-}$ (n = 18), at 30 hpf.

494 (E'') Graph of PHBC filopodia length in sib (n = 50) and *neurog1*$^{-/-}$ (n = 48), at 30 hpf.

495

496 Scale bars, 50 µm in A and 20 µm in D,E. Error bars, mean ± SEM. Unpaired two-tailed
497 Student's *t*-test for B, C, D', E' and unpaired one-tailed Student's *t*-test for E''. * $p < 0.05$, ** p
498 < 0.01, *** $p < 0.001$. ns, non-significant. PHBC, primordial hindbrain channel; LDA, lateral
499 dorsal aorta; AAs, aortic arches; PHS, primary head sinus; CtAs, central arteries; SAG,
500 statoacoustic ganglion; EC, endothelial cells; sib, siblings.

501

502

503 **Figure 4 Inhibition of cytoneme processes by Latrunculin B results in expansion of**
504 **neuroblasts.**

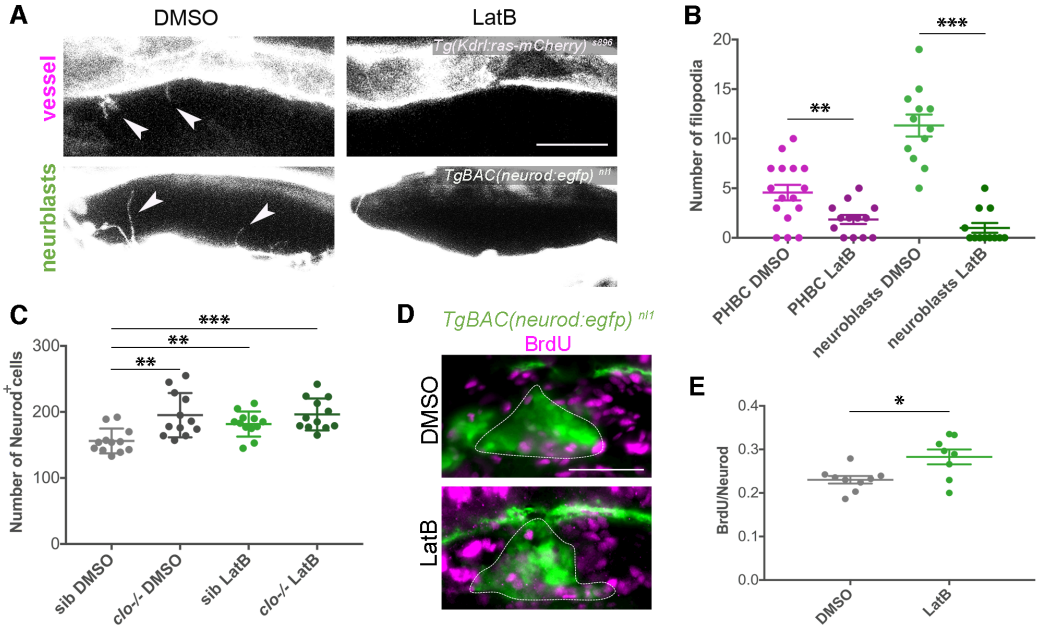

505

506 (A) Confocal lateral images showing filopodial processes in vessels and neuroblasts visualized
507 through *TgBAC(neurod:egfp)* ^{nl1} and *(Kdrl:ras-mCherry)* ^{s896} respectively, after 6h treatment in
508 DMSO or LatB, at 30 hpf. Arrowheads indicate filopodia.
509 (B) Quantification of filopodial processes number in vessels (n = 13-16) and neuroblasts (n =
510 12) after 6 hours incubation with LatB compared with control (DMSO), at 30 hpf.
511 (C) Graph showing the number of Neurod^{+} nuclei at 36 hpf, using the *TgBAC(neurod:egfp)* ^{nl1}
512 background and DAPI staining, in sib and clo $^{-/-}$ embryos treated with DMSO or LatB from 24-
513 30 hpf and washed until 36 hpf (n = 12).
514 (D) Lateral images of BrdU incorporation (magenta) in Neurod^{+} cells of the SAG (dotted line),
515 visualized through *TgBAC(neurod:egfp)* ^{nl1}, in 6 hours DMSO and LatB treated embryos, at 30
516 hpf.

(E) Graph showing the ratio of BrdU$^+$ cells in the Neurod$^+$ population after 6 hours DMSO (n = 9) and LatB (n = 8) treated embryos, at 30 hpf.

Scale bars, 20 µm in A and 50 µm in D. Error bars, mean ± SEM. In B,E unpaired two-tailed Student's *t*-test was performed. In C the data was analysed using one-way ANOVA, followed by post-hoc test. * $p < 0.05$, ** $p < 0.01$, *** $p < 0.001$. PHBC, primordial hindbrain channel; sib, siblings.

Figure 5 Down-regulation of Dll4 signalling induces neuroblast expansion.

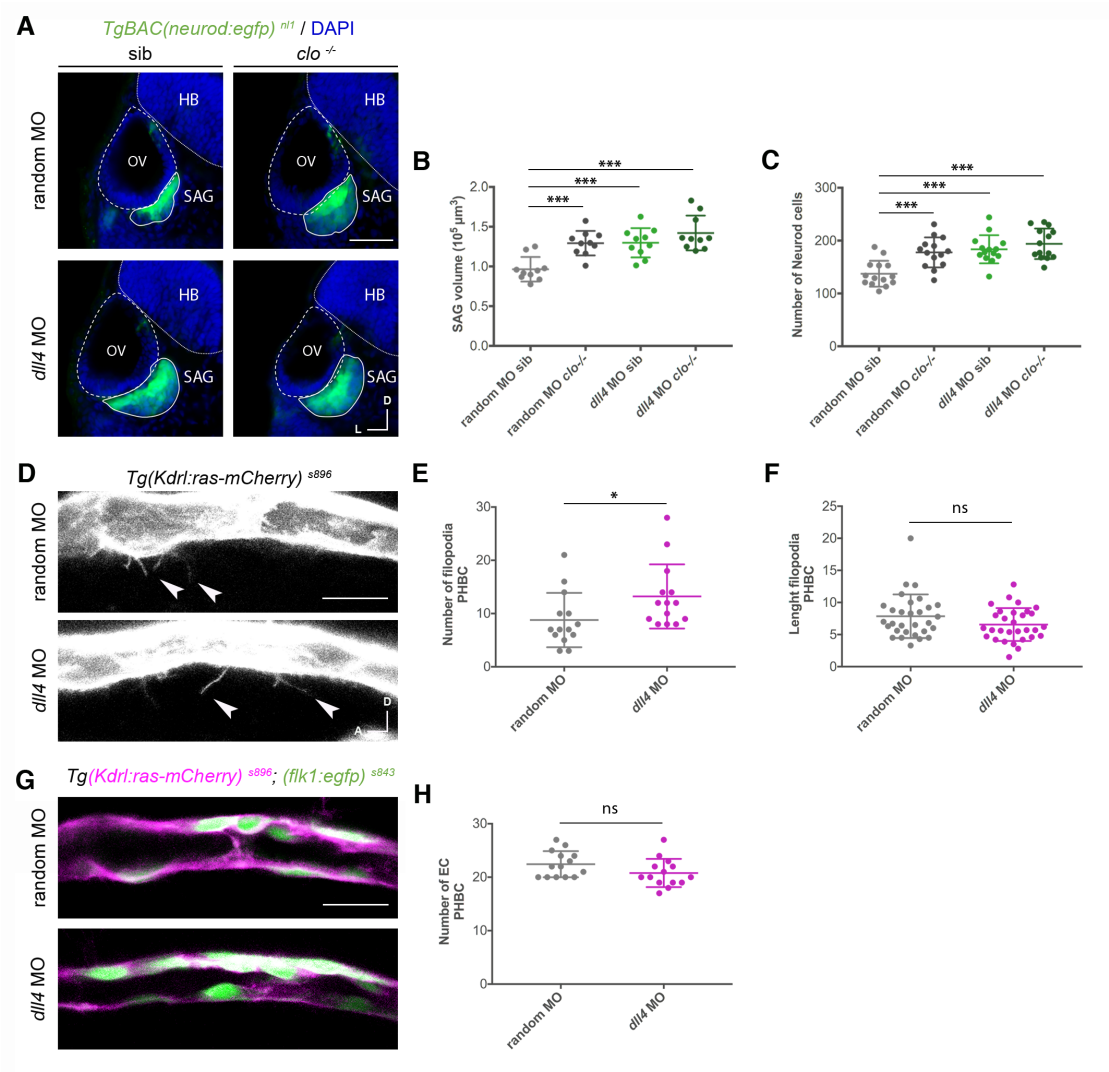

(A) Representative transverse sections showing the SAG in sib and clo$^{-/-}$ *TgBAC(neurod:egfp)* ^{nl1} embryos injected with of random or *dll4* splicing morpholino. Neurod$^+$ cells: green, neuroblasts; DAPI: blue, nuclei.

(B) Graph showing SAG volume quantification in sib and clo$^{-/-}$ embryos injected with random or *dll4* splicing morpholino (n = 10), at 36 hpf.

532 (C) Graph showing quantification of Neurod^{+} nuclei in sib and clo$^{-/-}$ embryos injected with
533 random or *dll4* splicing morpholino (n = 14), at 36 hpf.
534 (D) Confocal lateral images of PHBC filopodial processes in random and *dll4* morphants
535 visualized with the *Tg(Kdrl:ras-mCherry)*^{s896}, at 30 hpf. Arrowheads indicate filopodia.
536 (E,F) Quantification of PHBC filopodia number (n = 14) (E) and length (n = 14) (F), in random
537 and *dll4* morphants, at 30 hpf.
538 (G) Confocal lateral images showing EC membranes and cytoplasm using the *Tg(Kdrl:ras-*
539 *mCherry)*^{s896} and *Tg(flk1:egfp)*^{s843} respectively, in the PHBC, at 30 hpf.
540 (H) Quantification of EC number in random and *dll4* morphants (n = 14), at 30 hpf.
541
542 Scale bars, 50 µm in A, and 20 µm in D,G. Error bars, mean ± SEM. In B,C the data was analysed
543 using one-way ANOVA, followed by post-hoc test. In E the non-parametric Mann-Whitney *U*
544 test was performed. In F,H unpaired two-tailed Student's *t*-test was used. * $p < 0.05$, ** $p <$
545 0.01, *** $p < 0.001$. HB, hindbrain; OV, otic vesicle; SAG, statoacoustic ganglion; PHBC,
546 primordial hindbrain channel; EC, endothelial cell.
547
548 **Figure 6 Sensory neuronal differentiation requires blood vessels.**

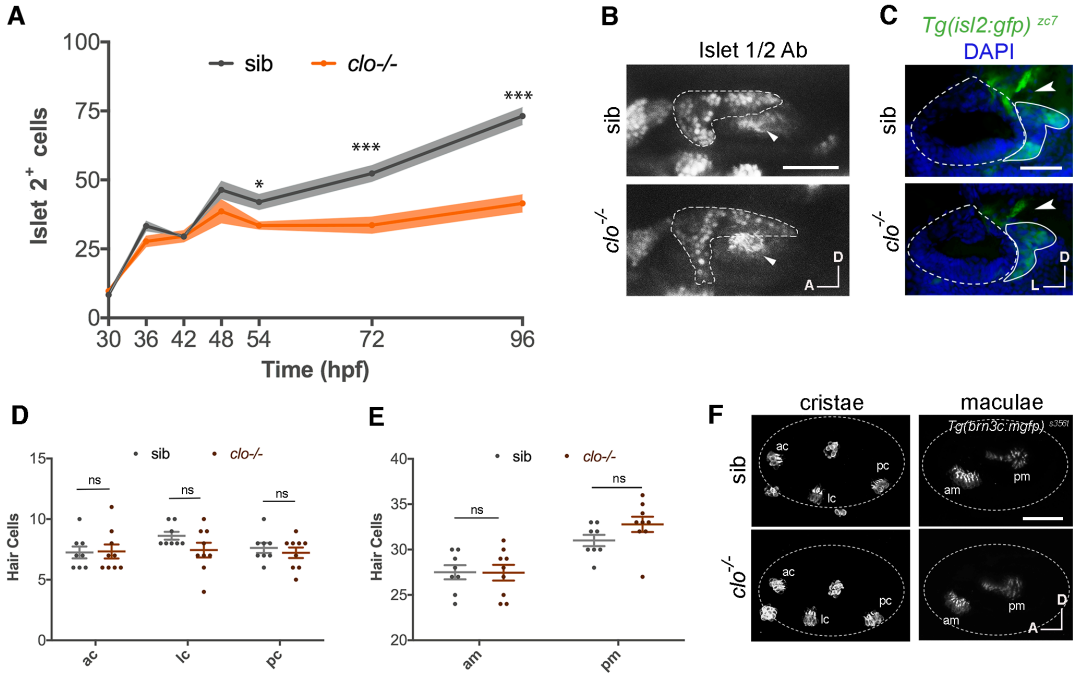

549
550 (A) Graph showing the number of Islet 2^{+} nuclei in the SAG at different timepoints from 30 to
551 96 hpf (n = 4-10).
552 (B) Confocal lateral images of immunostained Islet2^{+} nuclei in the SAG (dotted line, visualized
553 by *TgBAC(neurod:egfp)*^{nl1}) in sib and clo$^{-/-}$ embryos at 72 hpf. Arrowheads indicate pm.

554 (C) Transverse sections showing axon density (arrowhead) in the *Tg(isl2:gfp)* ^{zc7} in sib and clo^{-}
555 $^{/-}$ embryos, of cryostat sections, at 72 hpf. Dotted line indicates OV and continuous line the
556 SAG.
557 (D,E) Graph showing quantification of hair cell number in cristae (D) and maculae (E) in sib (n
558 = 8) and clo$^{-/-}$ (n = 9) embryos.
559 (F) Representative lateral images of hair cells in cristae and maculae using the *Tg(brn3c:mGFP)*
560 ^{s356t}, at 72 hpf. Dotted line indicates otic vesicle. Non-labelled hair cells are neuromasts.
561
562 Scale bars, 50 µm. Error bars, mean ± SD for A; and mean ± SEM for D,E. Unpaired two-tailed
563 Student's *t*-test. * $p < 0.05$, ** $p < 0.01$, *** $p < 0.001$. ns, non-significant. OV, otic vesicle;
564 SAG, statoacoustic ganglion; ac, anterior crista; lc, lateral crista; pc, posterior crista; am,
565 anterior macula; pm, posterior macula; sib, siblings.
566
567 **Figure 7 Blood flow triggers transcriptional changes related to oxygen sensing and**
568 **metabolism together with sensory neuronal differentiation in a restricted temporal**
569 **window.**

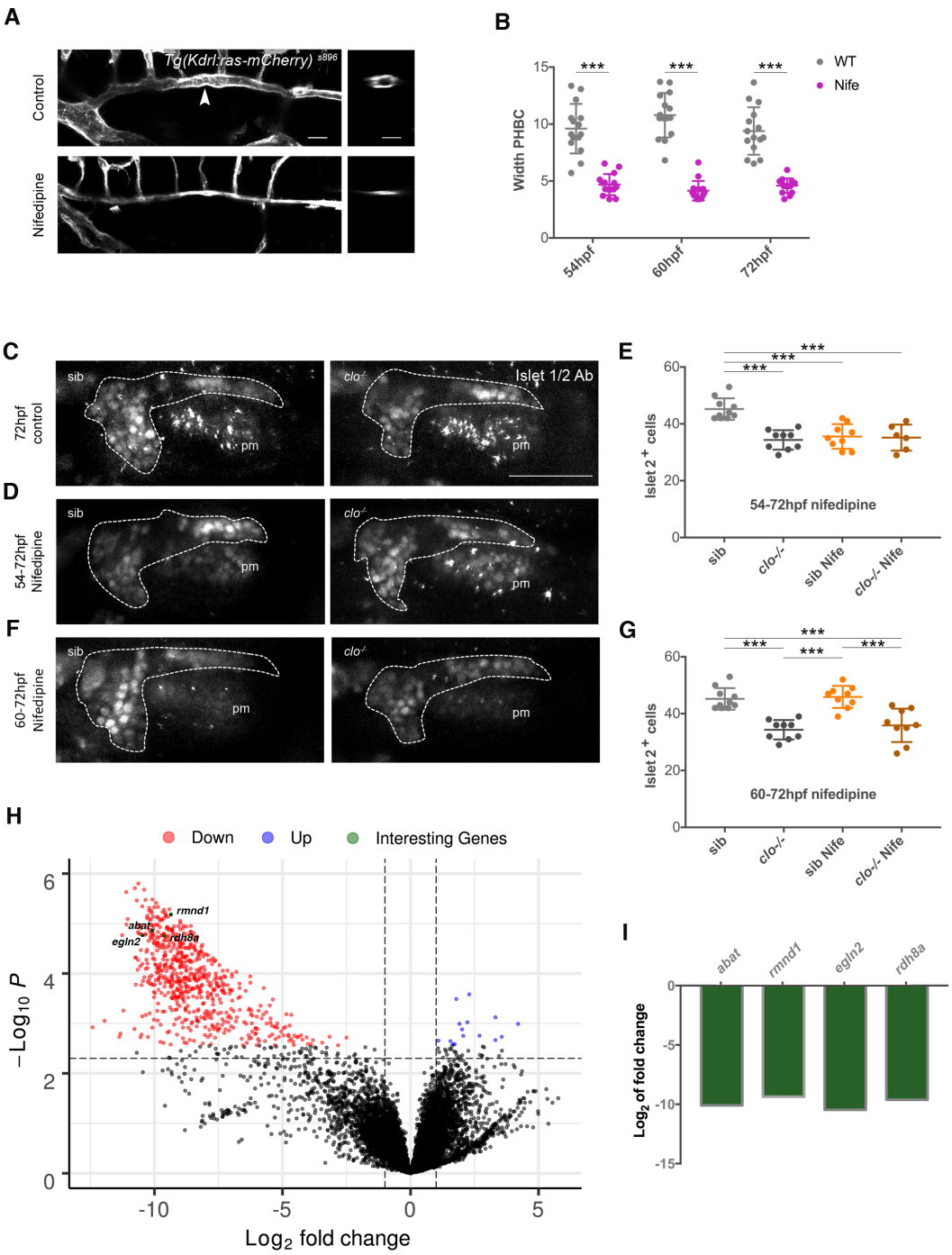

570

571 (A) Representative images of the PHBC of control and 48-54 hpf Nifedipine treated *Tg(Kdrl:ras-*

572 *mCherry)* ^{s896} embryos, at 54 hpf, in lateral (right) and transversal optic reconstructions (left)

573 in the point marked by the arrowhead.

574 (B) Analysis of PHBC width in control and Nifedipine treated *Tg(Kdrl:ras-mCherry)* ^{s896}

575 embryos, at 54, 60 and 72 hpf with treatment starting at 48 hpf (n=15).

576 (C-G) Confocal lateral images showing immunostained Islet2^{+} nuclei in the SAG (dotted line,

577 visualized by *Tg(neurod:egfp)* ^{nl1}) in sib and clo$^{-/-}$ embryos at 72 hpf in control (untreated) (C),

578 54-72 hpf Nifedipine treated embryos (D), 60-72 hpf Nifedipine treated embryos (F), and
579 quantified in E,G. 72 hpf sib (n = 10), 72 hpf clo$^{-/-}$ (n = 9), 54-72 hpf sib Nife (n = 9), 54-72 clo$^{-/-}$
580 Nife (n = 6), 60-72 hpf sib Nife (n = 9), 60-72 hpf clo$^{-/-}$ Nife (n = 9).
581 (H) Volcano plot of differentially expressed genes (DEGs) in the SAG at 54 hpf. Red and blue
582 plots represent significant downregulated and upregulated DEGs, respectively (P<0.05; FC<-
583 1; FC>1), while black plots represented insignificant DEGs (P≥0.05; FC≥-1; FC≤1). Genes of
584 special interest are highlighted in green.
585 (I) Histogram showing the fold change of DEGs of special interest in clo $^{-/-}$ versus sibling SAGs
586 at 54 hpf.
587
588 Scale bars, 50 µm for A,B,D,F, and 20 µm for H. Error bars, mean ± SEM. Unpaired two-tailed
589 Student's *t*-test. * p < 0.05, ** p < 0.01, *** p < 0.001. ns, non-significant. pm, posterior
590 macula; Nife, Nifedipine; sib, siblings; PHBC, primordial hindbrain channel.
591
592
593

594 ## STAR Methods

595 **Zebrafish Strains and Genotyping**

596 Zebrafish (*Danio rerio*) were maintained as previously described (Westerfield, 2000) at the
597 aquatic facility of the Parc de Recerca Biomèdica de Barcelona (PRBB). The following
598 transgenic lines in different combinations were used: *Tg(neurog1)* ^{hi1059} (Golling et al., 2002)
599 mutant to inhibit neurogenesis and *Tg(cloche)* ^{m378} (Stainier et al., 1996) as an avascular model.
600 Five different reporter lines were used: *Tg(Kdrl:ras-mCherry)* ^{s896} (Chi et al., 2008) and
601 *Tg(flk1:EGFP)* ^{s843} (Jin et al., 2005) for vessels , *TgBAC(neurod:EGFP)* ^{nl1} (Obholzer et al., 2008)
602 for neuroblasts, *Tg(isl2:gfp)* ^{zc7} (also called Isl3) (Pittman et al., 2008) for sensory differentiated
603 neurons and *Tg(brn3c:mGFP)* ^{s356t} (Xiao et al., 2005) for hair cells .
604 Embryos were staged as previously described (Kimmel et al., 1995). Adult heterozygous for
605 *neurog1* ^{hi1059} allele were identified by PCR genotyping by fin-clip genomic DNA(Golling et al.,
606 2002). Homozygous *neurog1* mutant embryos were recognized by the significant reduction of
607 GFP signal in *Tg(neurog1)* ^{hi1059}, *BAC(neurod:EGFP)* ^{nl1}, *(Kdrl:ras-mCherry)* ^{s896} background.
608 Avascular mutants were identified by the lack of vasculature in the reporter line for
609 endothelial cells *Tg(Kdrl:ras-mCherry)* ^{s896} or *Tg(flk-1:EGFP)* ^{s843}, lack of blood cells and
610 circulation (visible under scope from 30-36hpf) and atrium enlargement, as described by
611 Stainer et al. (Stainier et al., 1995).

612 In both cases, wild-type and heterozygous-deficient siblings were undistinguishable and both
613 have been used and referred as siblings (sib). Finally, since *clo* mutant embryos die around
614 7dpf (Stainier et al., 1996), we studied embryos until 4 dpf to exclude vessel directed effects
615 from embryonic morbidity.
616
617 **Live imaging, confocal microscopy and quantifications**
618 Images of cryosections were acquired with a Leica DFC 7000 T microscope, and 40x oil
619 immersion (0.75 NA).
620 Whole-mount embryos imaging was performed on a Leica SP8 confocal microscope, with 20x
621 glycerol immersion lens (0.7 NA). Embryos were mounted in 1% low-melting agarose
622 (Ecogene) in PBS or Danieau's solution, for fixed and life embryos respectively, and placed
623 onto a glass-bottom dish. For life embryos, 0.1% Tricaine (Sigma) was also added. The 488-
624 and 561-nm laser lines were employed at a scan speed of 600 Hz.
625 For time-lapse imaging of filopodial, the resonant mode (8000 Hz) was used to achieve a high
626 spatiotemporal resolution. Frames were captured simultaneously with 488 nm and 561 nm
627 lasers at a time interval of 15 seconds. Z-size of 2 µm was used for videos and 0.5 µm for static
628 stacks and transverse optical reconstructions. Confocal stacks and movies were flattened by
629 maximum projections using FIJI (Image J).
630 Measurements were done manually with FIJI (Image J) for SAG and PHBC filopodia number,
631 length and orientation using one single static image, from a defined region of interest (ROI).
632 PHBC width was measured from maximum projection confocal images always at the same
633 point, between CtA 2 and 3. PHBC EC number was calculated by perinuclear green cytosolic
634 signalling from *Tg(flk-1:EGFP)* ^{s843} and EC contours from *Tg(Kdrl:ras-mCherry)* ^{s896} in a defined
635 ROI. When ROIs were used, the same area was used to compare samples. SAG anteroposterior
636 (AP) and dorsoventral (DV) axes length were measured from maximum projection confocal
637 lateral images. The mediolateral (ML) SAG axis was calculated from 5 serial cryosections, in
638 which the biggest measurement was used.
639 The number of Neurod^{+} nuclei was counted manually using DAPI staining in the
640 *TgBAC(neurod:egfp)* ^{nl1} labelled cells. *neurog1*$^{+}$ cells were also counted manually after an ISH
641 and DAPI staining. The number of HC was calculated using the *Tg(brn3c:mGFP)* ^{s356t} and
642 counting kinocilia number.
643 The volume of the SAG was measured by calculating the area the 5 serial cryosections that
644 include all SAG and multiplying them with each section thickness (20µm).
645

646 **Statistical Analysis**

647 All the data in the work were first tested for normal distribution using the Kolmogorov-
648 Smirnov test and the Levene's test for homogeneity of variances. For two-group comparison
649 two-tailed Student's *t*-test was used or Mann-Whitney *U* test for non-parametric tests. When
650 more than two samples were being compared, one-way ANOVA followed by post-hoc test was
651 performed. Values are expressed as median ± SEM. Graphs were performed with PRISM 7
652 (Graph-Pad) software. Error bars represent SEM, but for Fig. 2d and Fig. 5a, were shaded error
653 bars represent SD. ns= non-significant, *p≤0.05, **p≤0.01, ***p≤0.001.

654

655 **Immunostaining and *in situ* Hybridization**

656 Embryos at the desired stage were fixed with 4% paraformaldehyde (PFA) in PBS 0,1% Tween-
657 20 (PBT) for 3 hours at RT or overnight at 4ºC. Fixed embryos were dehydrated, kept in 100%
658 MeOH -20ºC 1h or overnight (O/N), and rehydrated. Embryos were permeabilized with
659 Proteinase K 1:1000 in PBT, or cold Acetone for mouse anti-Islet1/2, and incubated with
660 blocking solution (BS) for 2h at room temperature (RT) and with primary antibody O/N at 4ºC.
661 Primary antibody was washed 5 times 10min, and secondary antibody was applied for 2h RT
662 or O/N 4ºC.

663 Embryos were cryoprotected in 15% sucrose and embedded in 7.5% gelatine/15% sucrose.
664 Blocks were frozen in 2-methylbutane (Sigma) to improve tissue preservation. Sagittal and
665 transversal sections were cut at 20µm thickness in a Leica CM 1950 cryostat.

666 For BrdU incorporation experiments, dechorionated live embryos were incubated with 10mM
667 BrdU, 10% DMSO in Danieau's solution for 6 hours. After this they were washed twice in clean
668 Danieau's solution for 5 min prior 4% PFA fixation for 3 hours at RT. BrdU staining was
669 performed in cryosections after 2N HCl DNA denaturation 1h RT. Anti-BrdU (bdbiosciences;
670 mouse Cat: 555627, 1:100). Anti-GFP was used to enhance GFP signal from transgenic lines
671 (Torrey Pines BioLabs Inc; rabbit Cat: TP401, 1:400). Anti-Islet1/2 was used to detect
672 differentiated neurons (Cat: TP401; mouse Cat: 39.4D5, 1:200). Alexa-fluor 488 and 594 anti-
673 rabbit and anti-mouse (Invitrogen, 1:400) were used as secondary antibodies. DAPI staining
674 for cryosections was done at 1:10000 PBS for 5min, and 2x5min wash in PBS followed by
675 mowiol mounting.

676 Whole-mount *in situ* hybridization was performed as previously described (Thisse et al., 2004)
677 using *neurog1* digoxigenin-labelled probe.

678

679

680 **Inhibitor treatments**

681 To block actin polymerization in filopodia, dechorionated live embryos were incubated in
682 0,1µg/mL Latrunculin B (LatB) (Merk, Millipore), 0,4% DMSO in Danieau's solution for 6 hours
683 (Phng et al., 2013); while control embryos were raised at 0,4% DMSO only. After treatment,
684 embryos were washed twice in clean Danieau's solution for 5min followed by immediate
685 confocal imaging for filopodia visualization or 4% PFA fixation. In other cases, embryos were
686 washed in Danieau's solution until 36 hpf. It has been previously demonstrated that the
687 concentration used of LatB specifically inhibits filopodial formation while it does not affect
688 other cellular behaviours for up to 17 hours of treatment (Phng et al., 2013).
689 Blood flow was blocked through the use of two different drugs. Dechorionated live embryos
690 were incubated for 6, 12 and 24 hours in 40µM Nifedipine or 20mM BDM (2, 3-butanedione-
691 2-monoxime) (Sigma-Aldrich) in Danieau's solution, washed twice 5min and fixed in 4% PFA
692 at the desired stage (Anderson et al., 2008; Li et al., 2008).
693

694 **Morpholino knockdown experiments**

695 To inhibit protein translation of Dll4, 10ng of random and *dll4* splicing morpholino antisense
696 oligonucleotides (Gene Tools, Philomath, OR) were injected in the yolk of 1-2 cell stage
697 embryos as previously described (Siekmann and Lawson, 2007). Efficiency of the knockdown
698 was assessed by RT-PCR (data not shown).
699

700 **FACS purification of GFP$^+$ cells**

701 Embryos of the transgenic line *Tg(neurod:gfp)* ^{nl1} were grown until 54 hpf, stage at which they
702 were anesthetized with tricaine. The SAG was dissected cutting the embryos head after the
703 eye and in the posterior end of the otic vesicle. The hindbrain was also removed to prevent
704 the sorting of any neurod$^+$ cells also present in the CNS. The presence of the SAG was
705 confirmed under a fluorescent scope. The dissected tissue was kept in Medium 199, on ice,
706 until we summed around 60 embryos per each condition siblings and *clo*. Cell were
707 disaggregated using a protease solution (10x Trypsin, 0,5M EDTA, 1x PBS) for 20 min with
708 mechanical help by both vortexing and doing up&down with a 200 µL pipete. Cell
709 disaggregation was stopped with STOP solution (30% FBS, 2M CaCl2, 1x PBT). Cells were
710 recovered by centrifugation and re-suspended in cell suspension medium (20% BSA, 0,5M
711 EDTA, 1x PBS). Neurod$^+$ cells were FACS purified based on GFP fluorescence utilizing a INFLUX
712 Sorter. Dead cells were eliminated by DAPI staining (1:1000). Cells were collected in collection
713 medium (1:1, PBS:FBS) and immediately used to RNA extraction.

714 Four replicates were used, always preparing one sample for siblings and another for *clo*
715 mutants each time, coming from the same breed.
716
717 **RNA extraction and sequencing**
718 RNA-seq was performed on FACS-sorted neuroblasts from the *Tg(neurod:egfp)* ^{nl1} zebrafish
719 embryos at 54 hpf. RNA from these cells was extracted using the PicoPure™ RNA Isolation
720 Kit (Thermo Fisher, KIT0214).
721 Cells from around 60 embryos were pooled to obtain enough RNA for library preparation.
722 cDNA was prepared with SMART-Seq® v4 Ultra® Low Input RNA Kit for Sequencing (Takara,
723 634888) and validated using Bioanalyzer High Sensitivity DNA Kit (Agilent, Cat. No. 5067-
724 4626). Between 66-306 pg of these cDNAs were used to prepare libraries using Nextera XT
725 DNA Library Prep Kit (Illumina, FC-131-1024). Libraries were validated using Bioanalyzer High
726 Sensitivity DNA Kit (Agilent, Cat. No. 5067-4626). Then, libraries were normalized and pooled
727 for sequencing using the NextSeq High Output (Illumina, 20024907) with 75 bp paired ends
728 run with 50 million expected reads per sample.
729 Mapped reads with the Zebrafish genome (version GRCz11) were obtained using the STAR
730 software (v2.5.2b, https://github.com/alexdobin/STAR), and the reads' counts within exons
731 with the HTSeq software (v0.9.1, https://htseq.readthedocs.io/en/release_0.11.1/). The DE
732 analysis was done with the limma package in R
733 (v3.38.3, https://bioconductor.org/packages/release/bioc/html/limma.html).
734

735 ## Supplemental Figures and Video Legends
736
737 **Figure S1 Protocol used for quantification of Neurod⁺ cell number.**

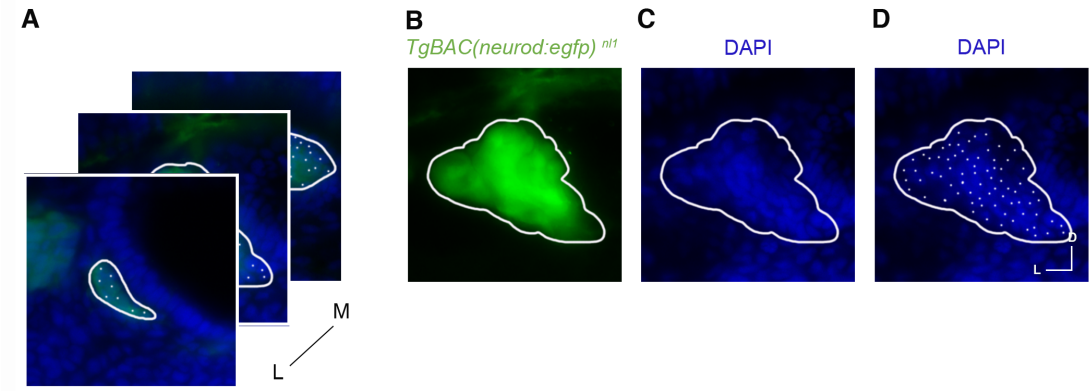

738
739 (A-C) For a series of latero-medial in sagittal or antero-posterior transversal (data not shown)
740 cryostat sections, the perimeter of the SAG was drawn using the green signal of

TgBAC(neurod:egfp) nl1 (B), subsequently green light was hidden and blue light from DAPI staining was visualized (C) to manually count the number of cells (D).

Figure S2 EC from the PHBC and neuroblasts from the SAG extend filopodia towards each other from 24 to 36 hpf.

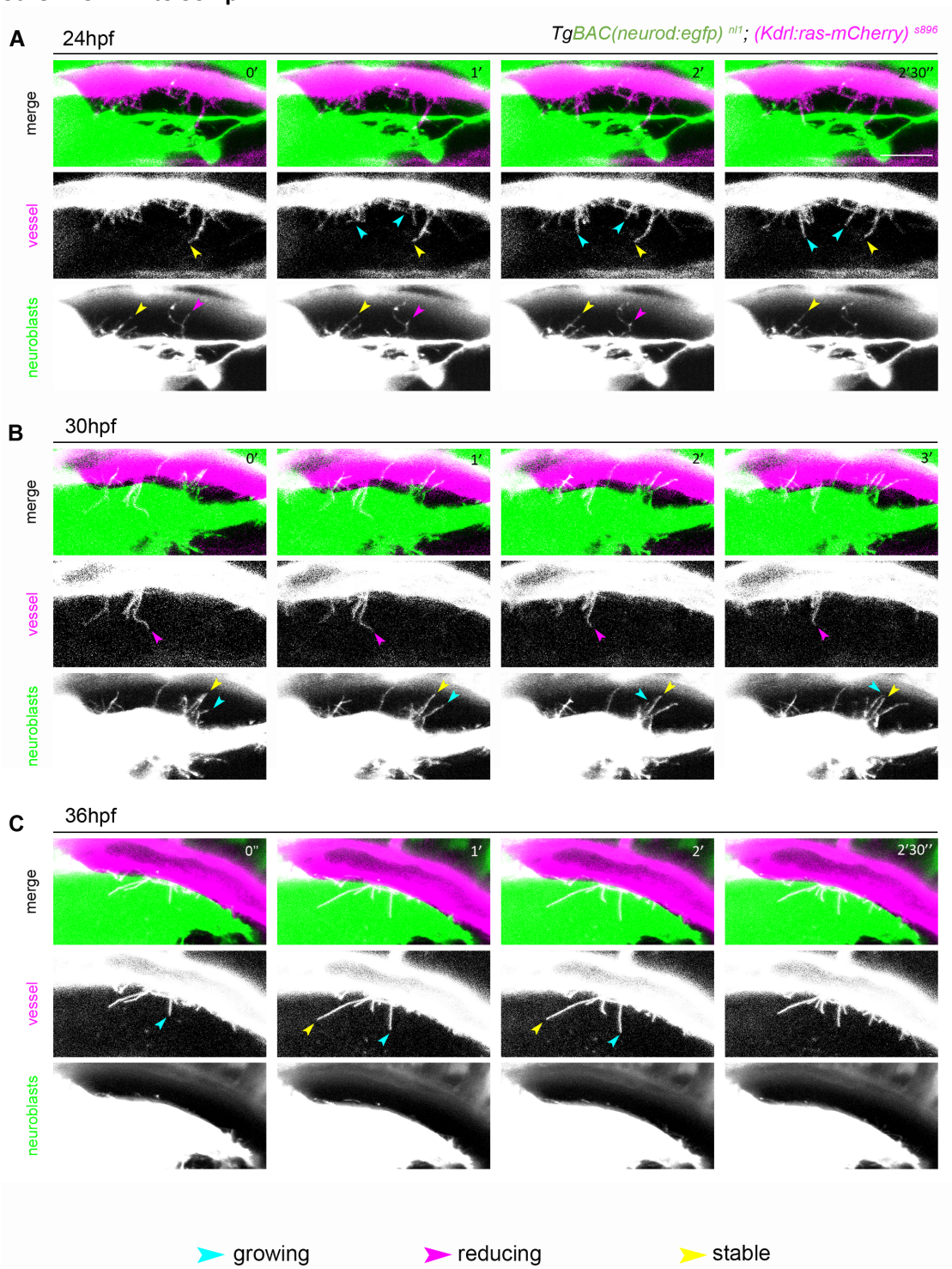

(A-C) Still images of time-lapse videos of *TgBAC(neurod:egfp)* ^{nl1}; *(Kdrl:ras-mCherry)* ^{s896} showing filopodia extending from the PHBC to neuroblasts and from neuroblasts to PHBC at 24 hpf (A), 30 hpf (B), and 36 hpf (C) (time-lapses are representative of 5 experiments), in a lateral view.

752 Cyan, magenta and yellow arrowheads point to examples of growing, reducing and stable
753 filopodia, respectively.
754
755 Scale bar 50 µm. PHBC, primordial hindbrain channel.
756
757 **Figure S3 Filopodia from vasculature and neuroblasts contact each other at the same plane.**

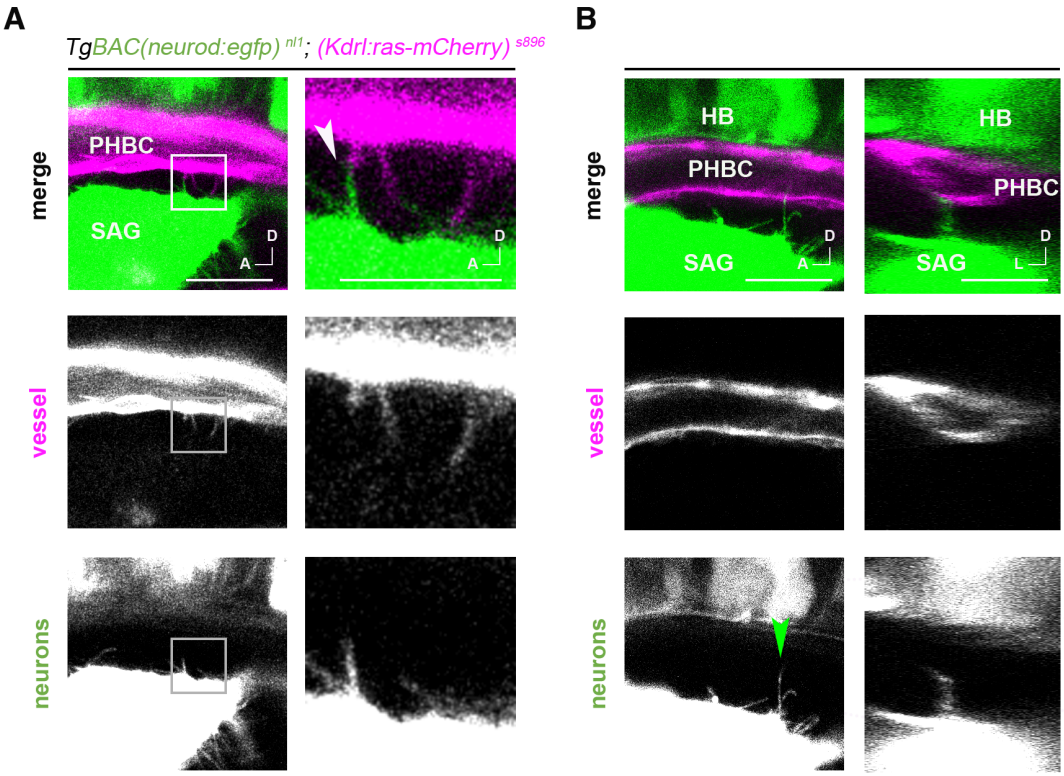

758
759 (A) Confocal lateral image of a single plane showing a filopodia-filopodia contact between EC
760 and neuroblasts. Square shows magnified image in the right, and arrowhead the mentioned
761 contact.
762
763 (B) Confocal lateral image of a single plane and transverse optical reconstruction also in single
764 plane showing a filopodial process from the neuroblasts contacting the EC. Arrowhead
765 indicates point for transverse optical reconstruction.
766
767 Scale bar 20 µm. PHBC, primordial hindbrain channel; SAG, statoacoustic ganglion; HB,
768 hindbrain.
769
770
771 **Figure S4 Filopodial contacts and defects on sensory neurogenesis in absence of vasculature**
772 **in other sensory ganglia.**

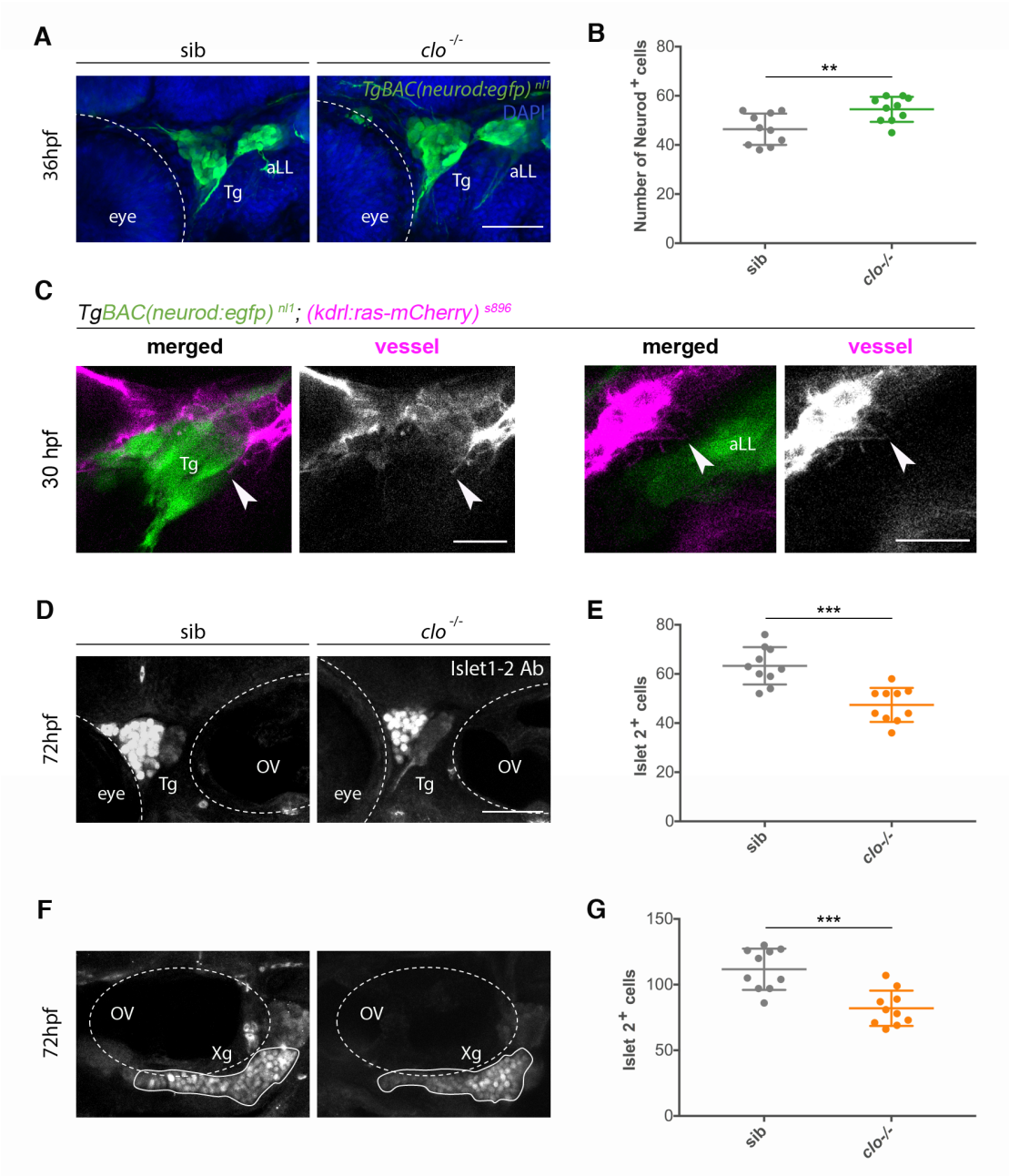

(A) Confocal lateral images of Tg and aLL ganglia in sib and clo$^{-/-}$ *TgBAC(neurod:egfp)* ^{nl1} embryos, at 36 hpf. Neurod^{+} cells: green, neuroblasts; DAPI: blue, nuclei.

(B) Quantification of Neurod^{+} cells in the Tg of sib and clo$^{-/-}$ embryos, at 36 hpf (n = 10).

(C) Confocal lateral images of a single plane showing filopodial processes from the PHBC contacting neuroblasts of the Tg and aLL ganglia. Arrowheads indicate filopodia.

(D-G) Confocal lateral images showing the number of Islet2^{+} nuclei in the Tg (c) and Xg ganglia (e) through Islet 1/2 antibody staining and quantified in E and G respectively (n = 10), at 72 hpf.

Scale bars 50 µm for A, B, D-G, and 20 µm for C. Error bars, mean ± SEM. Unpaired two-tailed Student's t-test. * $p < 0.05$, ** $p < 0.01$, *** $p < 0.001$. ns, non-significant. Tg, Trigeminal ganglion; aLL, anterior Lateral Line, OV, Otic Vesicle; Xg, Vagus ganglion; sib, siblings.

Figure S5 Blood flow arrest by Nifepidine at 60-72 hpf does not affect neuronal differentiation, while BDM at 54-72 hpf does.

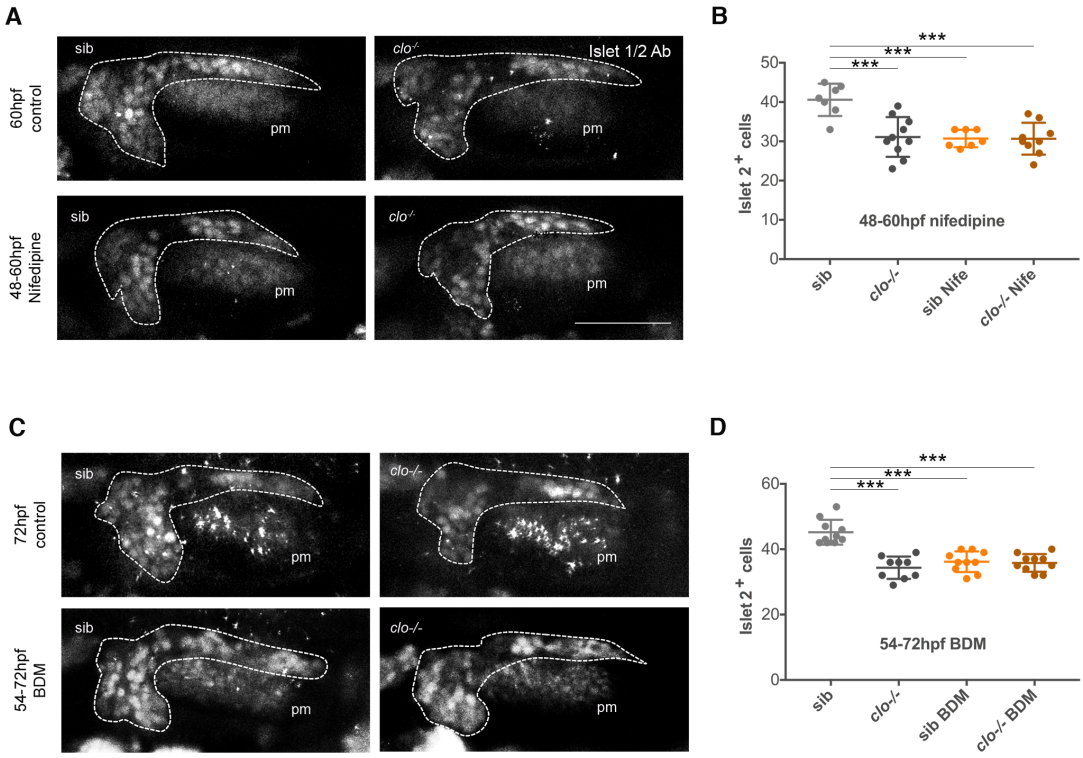

(A,B) Confocal images showing immunostained Islet2^{+} nuclei in the SAG (dotted line, visualized by *TgBAC(neurod:egfp)* ^{nl1}) at 60 hpf in control (untreated) and 48-60 hpf Nifedipine treated sib and clo$^{-/-}$ embryos; and quantified in I. 60 hpf sib (n = 7), 60 hpf clo$^{-/-}$ (n = 10), 48-60 hpf sib (n = 7), 48-60 hpf clo$^{-/-}$ (n = 9).

(C) Confocal lateral images showing immunostained Islet2^{+} nuclei in the SAG (dotted line, visualized by *TgBAC(neurod:egfp)* ^{nl1}) in sib and clo$^{-/-}$ embryos at 72 hpf in control (untreated) and 54-72 hpf BDM treated embryos.

(D) Graph showing the number of Islet 1/2^{+} cells in sib (n = 10), clo-/- (n = 9), 54-72 hpf sib BDM (n = 10), and 54-72 hpf clo$^{-/-}$ BDM (n = 10).

Scale bar 50 µm. Error bars mean ± SEM. Unpaired two-tailed Student's t-test. * $p < 0.05$, ** $p < 0.01$, *** $p < 0.001$. ns, non-significant. pm, posterior macula; sib, siblings.

Movie S1 Filopodial processes of the endothelial cells and neuroblasts contact each other at 30 hpf.

Z-projection time-lapse video of *TgBAC(neurod:egfp)* ^{nl1}; *(Kdrl:ras-mCherry)* ^{s896} embryos showing filopodia extending from the PHBC to the SAG and from the SAG to the PHBC at 30 hpf. Note thickenings in some neuroblasts filopodial. Lateral view. Scale bar 10 µm.

Movie S2 Filopodial processes of the endothelial cells and neuroblasts contact each other at 30 hpf.

820
821 Z-projection time-lapse video of *TgBAC(neurod:egfp)* ^{nl1}; *(Kdrl:ras-mCherry)* ^{s896} embryos
822 showing filopodia extending from the PHBC to the SAG and from the SAG to the PHBC at 30
823 hpf. Note dynamism of filopodial processes. Lateral view. Scale bar 10 µm.
824
825 **Movie S3 Filopodial processes of the endothelial cells and neuroblasts contact each other**
826 **at 36 hpf.**
827
828 Z-projection time-lapse video of *TgBAC(neurod:egfp)* ^{nl1}*; (Kdrl:ras-mCherry)* ^{s896} embryos
829 showing filopodia extending from the PHBC to the SAG and from the SAG to the PHBC at 36
830 hpf. Note dynamics of filopodial processes. Lateral view. Scale bar 10 µm.
831
832
833 **Movie S4 Filopodial processes of the endothelial cells and neuroblasts contact each other**
834 **at 36 hpf.**
835
836 Z-projection time-lapse video of *TgBAC(neurod:egfp)* ^{nl1}*; (Kdrl:ras-mCherry)* ^{s896} embryos
837 showing filopodia extending from the PHBC to the SAG and from the SAG to the PHBC at 36
838 hpf. Note length of EC filopodia. Lateral view. Scale bar 10 µm.
839

840 ## References

841 Adamo, L., Naveiras, O., Wenzel, P.L., McKinney-Freeman, S., Mack, P.J., Gracia-Sancho, J.,
842 Suchy-Dicey, A., Yoshimoto, M., Lensch, M.W., Yoder, M.C., et al. (2009). Biomechanical
843 forces promote embryonic haematopoiesis. Nature *459*, 1131–1135.
844 Alsina, B., Giraldez, F., and Varela-Nieto, I. (2003). Growth Factors and Early Development of
845 Otic Neurons: Interactions between Intrinsic and Extrinsic Signals. Curr. Top. Dev. Biol. *57*,
846 177–206.
847 Anderson, M.J., Pham, V.N., Vogel, A.M., Weinstein, B.M., and Roman, B.L. (2008). Loss of
848 unc45a precipitates arteriovenous shunting in the aortic arches. Dev. Biol. *318*, 258–267.
849 Androutsellis-Theotokis, A., Rueger, M.A., Park, D.M., Mkhikian, H., Korb, E., Poser, S.W.,
850 Walbridge, S., Munasinghe, J., Koretsky, A.P., Lonser, R.R., et al. (2009). Targeting neural
851 precursors in the adult brain rescues injured dopamine neurons. Proc. Natl. Acad. Sci. *106*,
852 13570–13575.
853 Barber, M., Andrews, W.D., Memi, F., Gardener, P., Ciantar, D., Tata, M., Ruhrberg, C., and
854 Parnavelas, J.G. (2018). Vascular-derived VEGFA promotes cortical interneuron migration
855 and proximity to the vasculature in the developing forebrain. Cereb. Cortex *28*, 2577–2593.
856 Begbie, J., Ballivet, M., and Graham, A. (2002). Early Steps in the Production of Sensory
857 Neurons by the Neurogenic Placodes. Mol. Cell. Neurosci. *21*, 502–511.
858 Bilak, M.M., Hossain, W.A., and Morest, D.K. (2003). Intracellular fibroblast growth factor
859 produces effects different from those of extracellular application on development of avian

860 cochleovestibular ganglion cells in vitro. J. Neurosci. Res. *71*, 629–647.
861 Bonapace, G., Concolino, D., Formicola, S., and Strisciuglio, P. (2003). A novel mutation in a
862 patient with insulin-like growth factor 1 (IGF1) deficiency. J Med Genet. *40*, 913–917.
863 Bussmann, J., Wolfe, S.A., and Siekmann, A.F. (2011). Arterial-venous network formation
864 during brain vascularization involves hemodynamic regulation of chemokine signaling.
865 Development *138*, 1717–1726.
866 Calvo, C.F., Fontaine, R.H., Soueid, J., Tammela, T., Makinen, T., Alfaro-Cervello, C., Bonnaud,
867 F., Miguez, A., Benhaim, L., Xu, Y., et al. (2011). Vascular endothelial growth factor receptor
868 3 directly regulates murine neurogenesis. Genes Dev. *25*, 831–844.
869 Camarero, G., Leon, Y., Gorospe, I., De Pablo, F., Alsina, B., Giraldez, F., and Varela-Nieto, I.
870 (2003). Insulin-like growth factor 1 is required for survival of transit-amplifying neuroblasts
871 and differentiation of otic neurons. Dev. Biol. *262*, 242–253.
872 Chi, N.C., Shaw, R.M., Val, S. De, Kang, G., Jan, L.Y., Black, B.L., and Stainier, D.Y.R. (2008).
873 Foxn4 directly regulates tbx2b expression and atrioventricular canal formation. Genes Dev.
874 734–739.
875 Chiu, J.-J., and Chien, S. (2011). Effects of Disturbed Flow on Vascular Endothelium:
876 Pathophysiological Basis and Clinical Perspectives. Physiol. Rev. *91*, 327–387.
877 Cleaver, O., and Dor, Y. (2012). Vascular instruction of pancreas development. *2843*, 2833–
878 2843.
879 Cliff, T.S., and Dalton, S. (2017). Metabolic switching and cell fate decisions : implications for
880 pluripotency , reprogramming and development. Curr. Opin. Genet. Dev. *46*, 44–49.
881 Delgado, A.C., Ferrón, S.R., Vicente, D., Porlan, E., Perez-Villalba, A., Trujillo, C.M., D'Ocón,
882 P., and Fariñas, I. (2014). Endothelial NT-3 Delivered by Vasculature and CSF Promotes
883 Quiescence of Subependymal Neural Stem Cells through Nitric Oxide Induction. Neuron *83*,
884 572–585.
885 Du, Y., Zhang, S., Yu, T., Du, G., Zhang, H., and Yin, Z. (2016). Wnt3a is critical for endothelial
886 progenitor cell-mediated neural stem cell proliferation and differentiation. Mol. Med. Rep.
887 *14*, 2473–2482.
888 Epstein, A., Gleadle, J., McNeill, L., Hewitson, K., O'Rourke, J., Mole, D., Mukherji, M.,
889 Metzen, E., Wilson, M., Dhanda, A., et al. (2001). C . elegans EGL-9 and Mammalian
890 Homologs Define a Family of Dioxygenases that Regulate HIF by Prolyl Hydroxylation The
891 Henry Wellcome Building of Genomic Medicine. Cell *107*, 43–54.
892 Fantetti, K.N., and Fekete, D.M. (2012). Members of the BMP, Shh, and FGF morphogen
893 families promote chicken statoacoustic ganglion neurite outgrowth and neuron survival in

894 vitro. Dev. Neurobiol. *72*, 1213–1228.
895 Fantin, A., Lampropoulou, A., Gestri, G., Raimondi, C., Senatore, V., Zachary, I., and
896 Ruhrberg, C. (2015). NRP1 Regulates CDC42 Activation to Promote Filopodia Formation in
897 Endothelial Tip Cells. Cell Rep. *11*, 1577–1590.
898 Fuwa, T.J., Kinoshita, T., Nishida, H., and Nishihara, S. (2015). Reduction of T antigen causes
899 loss of hematopoietic progenitors in Drosophila through the inhibition of filopodial
900 extensions from the hematopoietic niche. Dev. Biol. *401*, 206–219.
901 Gerhardt, H., Golding, M., Fruttiger, M., Ruhrberg, C., Lundkvist, A., Abramsson, A., Jeltsch,
902 M., Mitchell, C., Alitalo, K., Shima, D., et al. (2003). VEGF guides angiogenic sprouting
903 utilizing endothelial tip cell filopodia. J. Cell Biol. *161*, 1163–1177.
904 Golling, G., Amsterdam, A., Sun, Z., Antonelli, M., Maldonado, E., Chen, W., Burgess, S.,
905 Haldi, M., Artzt, K., Farrington, S., et al. (2002). Insertional mutagenesis in zebrafish rapidly
906 identifies genes essential for early vertebrate development. Nat. Genet. *31*, 135–140.
907 González-Méndez, L., Seijo-Barandiarán, I., and Guerrero, I. (2017). Cytoneme-mediated cell-
908 cell contacts for Hedgehog reception. Elife *6*, 1–24.
909 Hamada, H., Watanabe, M., Lau, H.E., Nishida, T., Hasegawa, T., Parichy, D.M., and Kondo, S.
910 (2014). Involvement of Delta/Notch signaling in zebrafish adult pigment stripe patterning.
911 Development *141*, 318–324.
912 Hawkins, K., Joy, S., Delhove, J., Kotiadis, V., Fernandez, E., Fitzpatrick, L., Whiteford, J., King,
913 P., Bolanos, J., Duchen, M., et al. (2016). NRF2 Orchestrates the Metabolic Shift during
914 Induced Pluripotent Stem Cell Reprogramming Report NRF2 Orchestrates the Metabolic Shift
915 during Induced Pluripotent Stem Cell Reprogramming. Cell Rep. *14*, 1883–1891.
916 Himmels, P., Paredes, I., Adler, H., Karakatsani, A., Luck, R., Marti, H.H., Ermakova, O.,
917 Rempel, E., Stoeckli, E.T., and Ruiz De Almodóvar, C. (2017). Motor neurons control blood
918 vessel patterning in the developing spinal cord. Nat. Commun. *8*, 1–16.
919 Hogan, K.A., Ambler, C.A., Chapman, D.L., and Bautch, V.L. (2004). The neural tube patterns
920 vessels developmentally using the VEGF signaling pathway. Development *131*, 1503-13.
921 Homem, C.C.F., Steinmann, V., Burkard, T.R., Jais, A., and Esterbauer, H. (2014). Ecdysone
922 and Mediator Change Energy Metabolism to Terminate Proliferation in Drosophila Neural
923 Stem Cells. Cell *158*, 874–888.
924 Howe, D., Bradford, Y., Conlin, T., Eagle, A., Fashena, D., Frazer, K., Knight, J., Mani, P.,
925 Martin, R., Moxon, S., et al. (2013). ZFIN, the Zebrafish Model Organism Database: increased
926 support for mutants and transgenics.
927 Huang, H., and Kornberg, T.B. (2015). Myoblast cytonemes mediate Wg signaling from the

928 wing imaginal disc and Delta-Notch signaling to the air sac primordium. Elife *4*, 1–22.
929 Inaba, M., Buszczak, M., and Yamashita, Y.M. (2015). Nanotubes mediate niche-stem-cell
930 signalling in the Drosophila testis. Nature *523*, 329–332.
931 Ito, K., and Suda, T. (2014). Metabolic requirements for the maintenance of self-renewing
932 stem cells. Nat. Rev. Mol. Cell Biol. *15*, 243–256.
933 Jensen, R.W., Chuman, H., Trobe, J.D., and Deveikis, J.P. (2004). Facial and Trigeminal
934 Neuropathies in Cavernous Sinus Fistulas. J. Neuro-Ophthalmology *24*, 34–38.
935 Jin, K., Zhu, Y., Sun, Y., Mao, X.O., Xie, L., and Greenberg, D.A. (2002a). Vascular endothelial
936 growth factor (VEGF) stimulates neurogenesis in vitro and in vivo. Proc. Natl. Acad. Sci. *99*,
937 11946–11950.
938 Jin, K., Mao, X.O., Sun, Y., Xie, L., and Greenberg, D.A. (2002b). Stem cell factor stimulates
939 neurogenesis in vitro and in vivo. J. Clin. Invest. *110*, 311–319.
940 Jin, S.-W., Beis, D., Mitchell, T., Chen, J.-N., and Stainier, D.Y.R. (2005). Cellular and molecular
941 analyses of vascular tube and lumen formation in zebrafish. Development *132*, 5199–5209.
942 Kacem, K., Lacombe, P., Seylaz, J., and Bonvento, G. (1998). Structural Organization of the
943 Perivascular Astrocyte Endfeet and Their Relationship With the Endothelial Glucose
944 Transporter : A Confocal Microscopy Study. Glia *23*, 1–10.
945 Kida, Y., Kawamura, T., Wei, Z., Sogo, T., Jacinto, S., Shigeno, A., Kushige, H., Yoshihara, E.,
946 Liddle, C., Ecker, J., et al. (2015). ERRs Mediate a Metabolic Switch Required for Somatic Cell
947 Reprogramming to Pluripotency. Stem Cell *16*, 547–555.
948 Kimmel, C.B., Ballard, W.W., Kimmel, S.R., Ullmann, B., and Schilling, T.F. (1995). Stages of
949 Embryonic Development of the Zebrafish. Dev. Dyn. *203*, 253–310.
950 Kornberg, T.B. (2017). Distributing signaling proteins in space and time: the province of
951 cytonemes. Curr. Opin. Genet. Dev. *45*, 22–27.
952 Lago, M.R.R., Fernandes, L. da C., Lyra, I.M., Ramos, R.T., Teixeira, R., Salles, C., and Ladeia,
953 A.M.T. (2018). Sensorineural hearing loss in children with sickle cell anemia and its
954 association with endothelial dysfunction. Hematology *23*, 849–855.
955 Lange, C., Turrero Garcia, M., Decimo, I., Bifari, F., Eelen, G., Quaegebeur, A., Boon, R., Zhao,
956 H., Boeckx, B., Chang, J., et al. (2016). Relief of hypoxia by angiogenesis promotes neural
957 stem cell differentiation by targeting glycolysis. EMBO J. *35*, 924–941.
958 Leslie, J.D., Ariza-McNaughton, L., Bermange, A.L., McAdow, R., Johnson, S.L., and Lewis, J.
959 (2007). Endothelial signalling by the Notch ligand Delta-like 4 restricts angiogenesis.
960 Development *134*, 839–844.
961 Li, W.M., Webb, S.E., Chan, C.M., and Miller, A.L. (2008). Multiple roles of the furrow

962 deepening Ca2+ transient during cytokinesis in zebrafish embryos. Dev. Biol. *316*, 228–248.
963 Liao, W., Bisgrove, B., Sawyer, H., and Hug, B. (1997). The zebrafish gene cloche acts
964 upstream of a flk-1 homologue to regulate endothelial cell differentiation. Development
965 *124*, 381–389.
966 Llorens-Bobadilla, E., Zhao, S., Baser, A., Saiz-Castro, G., Zwadlo, K., and Martin-Villalba, A.
967 (2015). Single-Cell Transcriptomics Reveals a Population of Dormant Neural Stem Cells that
968 Become Activated upon Brain Injury. Cell Stem Cell *17*, 329–340.
969 Louissaint, A., Rao, S., Leventhal, C., and Goldman, S. (2002). Coordinated interaction of
970 neurogenesis and angiogenesis in the adult songbird brain. Neuron *34*, 945–960.
971 Ma, Q., Chen, Z., Barrantes, I. del B., Luis de la Pompa, J., and Anderson, D.J. (1998).
972 Neurogenin1 Is Essential for the Determination of Neuronal Precursors for Proximal Cranial
973 Sensory Ganglia. Neuron *20*, 469–482.
974 Maier, E.C., Saxena, A., Alsina, B., Bronner, M.E., and Whitfield, T.T. (2014). Sensational
975 placodes: Neurogenesis in the otic and olfactory systems. Dev. Biol. *389*, 50–67.
976 Makita, T., Sucov, H.M., Gariepy, C.E., Yanagisawa, M., and Ginty, D.D. (2008). Endothelins
977 are vascular-derived axonal guidance cues for developing sympathetic neurons. Nature *452*,
978 759–763.
979 Mandal, L., Martinez-Agosto, J.A., Evans, C.J., Hartenstein, V., and Banerjee, U. (2007). A
980 Hedgehog- and Antennapedia-dependent niche maintains Drosophila haematopoietic
981 precursors. Nature *446*, 320–324.
982 Mirzadeh, Z., Merkle, F.T., Soriano-Navarro, M., Garcia-Verdugo, J.M., and Alvarez-Buylla, A.
983 (2008). Neural Stem Cells Confer Unique Pinwheel Architecture to the Ventricular Surface in
984 Neurogenic Regions of the Adult Brain. Cell Stem Cell *3*, 265–278.
985 Mohrin, M., Shin, J., Liu, Y., Brown, K., Luo, H., Xi, Y., Haynes, C.M., and Chen, D. (2015). A
986 mitochondrial UPR-mediated metabolic checkpoint regulates hematopoietic stem cell aging.
987 Science (80-.). *347*, 1374-7.
988 Morton, W.M., Ayscough, K.R., and McLaughlin, P.J. (2000). Latrunculin alters the actin-
989 monomer subunit interface to prevent polymerization. Nat. Cell Biol. *2*, 376–378.
990 Mukouyama, Y., Shin, D., Britsch, S., Taniguchi, M., and Anderson, D.J. (2002). Sensory
991 Nerves Determine the Pattern of Arterial Differentiation and Blood Vessel Branching in the
992 Skin. Cell *109*, 693–705.
993 Murdoch, B., and Roskams, A.J. (2012). Fibroblast Growth Factor Signaling Regulates
994 Neurogenesis at Multiple Stages in the Embryonic Olfactory Epithelium. Stem Cells Dev. *22*,
995 525–537.

996 Nakajima, H., Yamamoto, K., Agarwala, S., Terai, K., Fukui, H., Fukuhara, S., Ando, K.,
997 Miyazaki, T., Yokota, Y., Schmelzer, E., et al. (2017). Flow-Dependent Endothelial YAP
998 Regulation Contributes to Vessel Maintenance. Dev. Cell *40*, 523-536.e6.
999 Nicoli, S., Standley, C., Walker, P., Hurlstone, A., Fogarty, K.E., and Lawson, N.D. (2010).
1000 MicroRNA-mediated integration of haemodynamics and Vegf signalling during angiogenesis.
1001 Nature *464*, 1196–1200.
1002 Nikolaou, N., Watanabe-Asaka, T., Gerety, S., Distel, M., Koster, R.W., and Wilkinson, D.G.
1003 (2009). Lunatic fringe promotes the lateral inhibition of neurogenesis. Development *136*,
1004 2523–2533.
1005 Le Noble, F., Klein, C., Tintu, A., Pries, A., and Buschmann, I. (2008). Neural guidance
1006 molecules, tip cells, and mechanical factors in vascular development. Cardiovasc. Res. *78*,
1007 232–241.
1008 Obernier, K., Cebrian-Silla, A., Thomson, M., Parraguez, J.I., Anderson, R., Guinto, C., Rodas
1009 Rodriguez, J., Garcia-Verdugo, J.M., and Alvarez-Buylla, A. (2018). Adult Neurogenesis Is
1010 Sustained by Symmetric Self-Renewal and Differentiation. Cell Stem Cell *22*, 221-234.e8.
1011 Obholzer, N., Wolfson, S., Trapani, J.G., Mo, W., Nechiporuk, A., Busch-Nentwich, E., Seiler,
1012 C., Sidi, S., Sollner, C., Duncan, R.N., et al. (2008). Vesicular Glutamate Transporter 3 Is
1013 Required for Synaptic Transmission in Zebrafish Hair Cells. J. Neurosci. *28*, 2110–2118.
1014 Ochsenbein, A.M., Karaman, S., Proulx, S.T., Berchtold, M., Jurisic, G., Stoeckli, E.T., and
1015 Detmar, M. (2016). Endothelial cell-derived semaphorin 3A inhibits filopodia formation by
1016 blood vascular tip cells. Development *143*, 589–594.
1017 Ottone, C., Krusche, B., Whitby, A., Clements, M., Quadrato, G., Pitulescu, M.E., Adams, R.H.,
1018 and Parrinello, S. (2014). Direct cell-cell contact with the vascular niche maintains quiescent
1019 neural stem cells. Nat. Cell Biol. *16*, 1045–1056.
1020 Palmer, T.D., Willhoite, A.R., and Gage, F.H. (2000). Vascular Niche for Adult Hippocampal
1021 Neurogenesis. J. Comp. Neurolgy *494*, 479–494.
1022 Paul, A., Mazighi, M., Lenck, S., Bresson, D., Herman, P., and Hautefort, C. (2016). Isolated
1023 intermittent bilateral hearing loss revealing a brain hemorrhage. J. Neurol. Sci. *370*, 18–20.
1024 Phng, L.-K., Stanchi, F., and Gerhardt, H. (2013). Filopodia are dispensable for endothelial tip
1025 cell guidance. Development *140*, 4031–4040.
1026 Pittman, A.J., Law, M.-Y., and Chien, C.-B. (2008). Pathfinding in a large vertebrate axon
1027 tract: isotypic interactions guide retinotectal axons at multiple choice points. Development
1028 *135*, 2865–2871.
1029 Rafii, S., Butler, J.M., and Ding, B. Sen (2016). Angiocrine functions of organ-specific

1030 endothelial cells. Nature *529*, 316–325.
1031 Ramasamy, S.K., Kusumbe, A.P., and Adams, R.H. (2015). Regulation of tissue morphogenesis
1032 by endothelial cell-derived signals. Trends Cell Biol. *25*, 148–157.
1033 Ramírez-Castillejo, C., Sánchez-Sánchez, F., Andreu-Agulló, C., Ferrón, S.R., Aroca-Aguilar,
1034 J.D., Sánchez, P., Mira, H., Escribano, J., and Fariñas, I. (2006). Pigment epithelium-derived
1035 factor is a niche signal for neural stem cell renewal. Nat. Neurosci. *9*, 331–339.
1036 Ramírez-Weber, F.-A., and Kornberg, T.B. (1999). Cytonemes: Cellular Processes that Project
1037 to the Principal Signaling Center in Drosophila Imaginal Discs. Cell *97*, 599–607.
1038 Reischauer, S., Stone, O.A., Villasenor, A., Chi, N., Jin, S.W., Martin, M., Lee, M.T., Fukuda, N.,
1039 Marass, M., Witty, A., et al. (2016). Cloche is a bHLH-PAS transcription factor that drives
1040 haemato-vascular specification. Nature *535*, 294–298.
1041 Riquelme, R., Cediel, R., Contreras, J., Rodríguez-de La Rosa, L., Murillo-Cuesta, S.,
1042 Hernandez, C., Zubeldia, J., Cerdan, S., and Varela-Nieto, I. (2010). A comparative study of
1043 age-related hearing loss in wild type and insulin-like growth factor I deficient mice. Front.
1044 Neuroanat. *4*, 27.
1045 Rojas-Ríos, P., Guerrero, I., and González-Reyes, A. (2012). Cytoneme-mediated delivery of
1046 Hedgehog regulates the expression of bone morphogenetic proteins to maintain germline
1047 stem cells in Drosophila. PLoS Biol. *10*, e1001298.
1048 Roy, S., Huang, H., Liu, S., and Kornberg, T.B. (2014). Cytoneme-mediated contact-dependent
1049 transport of the Drosophila decapentaplegic signaling protein. Science (80-.). *343*, 1244624.
1050 Ryall, J.G., Cliff, T., Dalton, S., and Sartorelli, V. (2015). Metabolic Reprogramming of Stem
1051 Cell Epigenetics. Cell Stem Cell *17*, 651–662.
1052 Sanders, T.A., Llagostera, E., and Barna, M. (2013). Specialized filopodia direct long-range
1053 transport of SHH during vertebrate tissue patterning. Nature *497*, 628–632.
1054 Schlosser, G. (2010). Making senses development of vertebrate cranial placodes. Int Rev Cell
1055 Mol Biol *283*, 129–234.
1056 Shen, Q., Wang, Y., Kokovay, E., Lin, G., Chuang, S.M., Goderie, S.K., Roysam, B., and Temple,
1057 S. (2008). Adult SVZ Stem Cells Lie in a Vascular Niche: A Quantitative Analysis of Niche Cell-
1058 Cell Interactions. Cell Stem Cell *3*, 289–300.
1059 Shi, S., and Gronthos, S. (2003). Perivascular Niche of Postnatal Mesenchymal Stem Cells in
1060 Human Bone Marrow and Dental Pulp. J. Bone Miner. Res. *18*, 696–704.
1061 Shi, X., Alves, T., Zeng, X.-L., Kibbey, R., Estes, M., and Guan, X. (2015). GLP-2 reprograms
1062 glucose metabolism in intestinal stem cells. FASEB J *29*, 851–854.
1063 Siekmann, A.F., and Lawson, N.D. (2007). Notch signalling limits angiogenic cell behaviour in

1064 developing zebrafish arteries. Nature *445*, 781–784.
1065 Siekmann, A.F., Standley, C., Fogarty, K.E., Wolfe, S.A., and Lawson, N.D. (2009). Chemokine
1066 signaling guides regional patterning of the first embryonic artery. Genes Dev. *23*, 2272–2277.
1067 Spradling, A., Drummond-Barbosa, D., and Kai, T. (2001). Stem cells find their niche. Nature
1068 *414*, 98–104.
1069 Stainier, D.Y., Weinstein, B.M., Detrich, H.W., Zon, L.I., and Fishman, M.C. (1995). Cloche, an
1070 early acting zebrafish gene, is required by both the endothelial and hematopoietic lineages.
1071 Development *121*, 3141–3150.
1072 Stainier, D.Y., Fouquet, B., Chen, J.N., Warren, K.S., Weinstein, B.M., Meiler, S.E., Mohideen,
1073 M.A., Neuhauss, S.C., Solnica-Krezel, L., Schier, A.F., et al. (1996). Mutations affecting the
1074 formation and function of the cardiovascular system in the zebrafish embryo. Development
1075 *123*, 285–292.
1076 Stanganello, E., and Scholpp, S. (2016). Role of cytonemes in Wnt transport. J. Cell Sci. *129*,
1077 665–672.
1078 Stanganello, E., Hagemann, A.I.H., Mattes, B., Sinner, C., Meyen, D., Weber, S., Schug, A.,
1079 Raz, E., and Scholpp, S. (2015). Filopodia-based Wnt transport during vertebrate tissue
1080 patterning. Nat. Commun. *6*, 1–14.
1081 Suchting, S., Freitas, C., le Noble, F., Benedito, R., Breant, C., Duarte, A., and Eichmann, A.
1082 (2007). The Notch ligand Delta-like 4 negatively regulates endothelial tip cell formation and
1083 vessel branching. Proc. Natl. Acad. Sci. *104*, 3225–3230.
1084 Sumanas, S., Jorniak, T., and Lin, S. (2005). Identification of novel vascular endothelial-
1085 specific genes by the microarray analysis of the zebrafish cloche mutants. Blood *106*, 534–
1086 541.
1087 Taberner, L., Bañón, A., and Alsina, B. (2018). Anatomical map of the cranial vasculature and
1088 sensory ganglia. J. Anat. *232*, 431–439.
1089 Tan, X., Liu, W.A., Zhang, X.J., Shi, W., Ren, S.Q., Li, Z., Brown, K.N., and Shi, S.H. (2016).
1090 Vascular Influence on Ventral Telencephalic Progenitors and Neocortical Interneuron
1091 Production. Dev. Cell *36*, 624–638.
1092 Tata, M., Wall, I., Joyce, A., Vieira, J.M., Kessaris, N., and Ruhrberg, C. (2016). Regulation of
1093 embryonic neurogenesis by germinal zone vasculature. Proc. Natl. Acad. Sci. *113*, 13414–
1094 13419.
1095 Tavazoie, M., Van der Veken, L., Silva-Vargas, V., Louissaint, M., Colonna, L., Zaidi, B., Garcia-
1096 Verdugo, J.M., and Doetsch, F. (2008). A Specialized Vascular Niche for Adult Neural Stem
1097 Cells. Cell Stem Cell *3*, 279–288.

1098 Thisse, B., Heyer, V., Lux, A., Alunni, V., Degrave, A., Seiliez, I., Kirchner, J., Parkhill, J.-P., and
1099 Thisse, C. (2004). Spatial and Temporal Expression of the Zebrafish Genome by Large-Scale In
1100 Situ Hybridization Screening. Methods Cell Biol. *77*, 505–519.
1101 Ulrich, F., Ma, L.H., Baker, R.G., and Torres-Vázquez, J. (2011). Neurovascular development
1102 in the embryonic zebrafish hindbrain. Dev. Biol. *357*, 134–151.
1103 Vasudevan, A., Long, J.E., Crandall, J.E., Rubenstein, J.L.R., and Bhide, P.G. (2008).
1104 Compartment-specific transcription factors orchestrate angiogenesis gradients in the
1105 embryonic brain. Nat. Neurosci. *11*, 429–439.
1106 Vemaraju, S., Kantarci, H., Padanad, M.S., and Riley, B.B. (2012). A Spatial and Temporal
1107 Gradient of Fgf Differentially Regulates Distinct Stages of Neural Development in the
1108 Zebrafish Inner Ear. PLoS Genet. *8*, e1003068.
1109 Westerfield, M. (2000). The zebrafish book. A guide for the laboratory use of zebrafish
1110 (Danio rerio). (Univ. of Oregon Press, Eugene.).
1111 Xiao, T., Roeser, T., Staub, W., and Baier, H. (2005). A GFP-based genetic screen reveals
1112 mutations that disrupt the architecture of the zebrafish retinotectal projection.
1113 Development *132*, 2955–2967.
1114 Yoshida, S., Sukeno, M., and Nabeshima, Y.I. (2007). A vasculature-associated niche for
1115 undifferentiated spermatogonia in the mouse testis. Science (80-.). *317*, 1722–1726.
1116
1117
1118
1119
1120